Impurity effects on semiconductor quantum bits in coupled quantum dots

Nga T. T. Nguyen and S. Das Sarma

Condensed Matter Theory Center, Department of Physics, University of Maryland, College Park, Maryland 20742-4111, USA

(Received 16 March 2011; revised manuscript received 27 April 2011; published 14 June 2011)

We theoretically consider the effects of having unintentional charged impurities in laterally coupled two-dimensional double (GaAs) quantum-dot systems, where each dot contains one or two electrons and a single charged impurity. Using molecular orbital and configuration interaction methods, we calculate the effect of the impurity on the two-electron energy spectrum of each individual dot as well as on the spectrum of the coupled-double-dot two-electron system. We find that the singlet-triplet exchange splitting between the two lowest-energy states, both for the individual dots and the coupled-dot system, depends sensitively on the location of the impurity and its coupling strength (i.e. the effective charge). A strong electron-impurity coupling breaks down the equality of the two doubly occupied singlets in the left and the right dots, leading to a mixing between different spin singlets. As a result, the maximally entangled qubit states are no longer fully obtained in the zero-magnetic-field case. Moreover, a repulsive impurity results in a triplet-singlet transition as the impurity effective charge increases or the impurity position changes. We comment on the impurity effect in spin qubit operations in the double-dot system based on our numerical results.

DOI: 10.1103/PhysRevB.83.235322 PACS number(s): 73.21.La, 78.67.Hc, 73.23.Hk, 03.67.Lx

I. INTRODUCTION

The goal of this paper is the calculation of the low-lying energy spectra of two-electron semiconductor quantum dots (QDs) (both single dots and coupled double dots) in the presence of nearby static-charged impurity centers within a minimal model. The purpose is to quantify the effects of quenched random-charged impurities on the singlet-triplet splitting in QDs in order to assess the importance of background unintentional impurities, which are invariably present in the environment, in adversely affecting the operations of exchange-coupled dots as elementary spin qubits for solid-state quantum computation. Since the positions and the strengths of the background unintentional impurities are unknown and random, we study the impurity effects as functions of impurity position and coupling strength (defined as the effective impurity charge Z), assuming the impurities to be Coulombic charge centers so that their effective potential falls off slowly as a $1/r$ potential away from the impurity location, where r is the distance from the impurity. Since the main background impurities in GaAs and Si, the two most relevant semiconductors of interest for solid-state spin quantum computations, are random-charge centers, our consideration of Coulombic impurities with a long-range impurity potential is reasonable. The theoretical results presented herein, while being completely microscopic and fully quantum mechanical, are phenomenological in nature since the impurity position and charge are treated as unknown parameters. While our results show clearly the strong effect of local background charged impurities on the low-lying QD spectra, their usefulness is limited in comparing with experiment since no direct information about impurity locations is currently available experimentally. On the other hand, our results establish the manifest importance of using the highest-quality background materials for semiconductor spin qubit operations since the presence of even a single charged impurity in the vicinity of the QDs seems to completely ruin the operational logistics of coupled QD systems. The exchange coupling (or equivalently, the singlet-triplet splitting) depends strongly and sensitively on the location and the strength of the charged impurity, which means that (1) a single charged impurity located nearby could destroy the qubit, and (2) even a remote charged impurity could have a strong adverse effect, inducing substantial qubit decoherence if the impurity is dynamic and has a fluctuation time scale comparable to gate operation time scales – in fact, the impurity-fluctuation time scale will become a dominant decoherence time since the exchange energy will vary substantially over this time scale. The motivation of our paper is a clear understanding of the energetics of QD systems in the few electron situations in the presence of charged impurities so that some rudimentary quantitative magnitudes of the impurity effects are available for qubit operation considerations.

Coupled QDs for quantum computation[1–5] have been extensively studied due to the prospect of using QDs as an ideal environment to confine and manipulate the QD electron spins. The quantum bit, or qubit, of information is encoded and stored in these localized single electron spins which exploit a spin relaxation time of the order of milliseconds,[6–8] sufficiently long to allow the performance of coherent spin operations. The proposed quantum computer[3] in solid states operates based on the exchange coupling J between the two-electron spin qubits manipulated by an external magnetic field. This exchange energy can be envisioned as the effective coupling between the two spins in the double dots[3] via the Heisenberg spin Hamiltonian, $\widehat{H} = J\mathbf{s}_1 \cdot \mathbf{s}_2$, which takes into account possible contributions from different hybridzations between singlet and triplet states. Hence J is determined through the gate voltage control over the tunneling coupling between the coupled two QDs. A complete understanding of J is important because it directly determines the $\sqrt{SWAP}$ operator which describes the exchange information between the two qubits in the double dots. The fast solid-state two-qubit operation,[3,9] generated as a consequence of the electron spin exchange under electrical control, and the single-qubit operation[10] suffice to assemble a standard quantum computing system. The number of electrons in such a QD system can be controlled precisely[11–14] to 0, and

the electron exchange interaction is tunable by the applied gate voltages; thereby the coupling between the dots can also be controlled.

Established quantum regimes such as quantum entanglement between individual electrons in one dot with the other electrons in the other dots and superposition of electron spin qubits are the major objects[3,4,9,15–25] in such exchange-coupled QD systems. Prerequisite criteria for realization of a quantum computation system[3] (including initialization, manipulation of spin qubits, and readout) have been demonstrated for single-dot[26] and coupled-QD systems,[27] and have provided the long relaxation time[6,14] of the spins by using charge-sensing and fast spin-to-charge conversion techniques. One of the perceived advantages of solid-state quantum computing is the scalability with existing semiconductors. In addition, integrating multicoupled dots into a quantum circuit is made possible by adding more suitable gate electrodes.[5,12]

QDs in versatile GaAs semiconductors not only have been considered the most widely studied objects in the QD science but also their well-understood physics is applicable to a variety of materials.[5] Often, unintentional impurities found in the dot sample are used in the fabrication process to adjust the potential-well height between different heterostructure semiconductors (such as Si in gated GaAs/AlGaAs QDs; see, e.g., Ref. 5), allowing the charge flow of electrons. Statistically, such a QD system containing impurities can be studied for one, two,. . ., impurities. On the other hand, when integrating multiple coupled two-dot systems utilized as a multi-qubit gate, in the nonoverlapping regime between different two-dot systems, a single spin qubit in one coupled two-dot system can be affected[28] by the other coupled two-dot systems. Each coupled two-dot system acts as a source of electrostatic field to the others and can be treated as "charged impurities."

Theoretical studies of impurities in coupled QDs have been rarely found in the literature. In fact, the impurities are practically found randomly in or outside the dot sample and their positions cannot be specified precisely. In a coupled-triple-dot system, a relatively large collection of impurities was considered.[29] These statistical impurities were theoretically assumed to induce a weak perturbation to the coupled triple QDs. The authors[29] found that the Coulomb exchange energy of the impurities with the QD electrons in this study resulted in decoherence of the coded qubit states. Thus any information processing using electron charge degrees of freedom needs to take into account the decoherence channel due to charge fluctuations.

In the present paper, we study the influence of charged impurities on the singlet-triplet splitting of the two lowest energy levels as well as the energy spectrum as a function of the impurity position, the impurity effective charge, and the number of impurities for a coupled-two-dot system in zero magnetic field. We also examine the impurity effect on the coupled-electron qubits by tuning the potential-well height to different values and obtain different triplet-singlet transitions for the repulsive impurity case. To accomplish, we discuss the singlet-triplet splitting in the presence of two impurities with similar charge located in the two separate dots of the system.

The paper is organized as follows. In Sec. II we introduce the model and methodology. The impurity effect on the energy spectrum of a two-electron single QD containing a single charged impurity is first discussed in detail in Sec. III. Section IV presents our studies on a coupled two-dot system in the presence of one or two charged impurities. We examine the impurity position and impurity effective-charge dependence of the singlet-triplet spin splitting energy. The influence of the confining potential barrier height on electron-impurity (e-I) and electron-electron (e-e) couplings is also explored. All the results presented in this paper are obtained at zero magnetic field, $B = 0$. A summary of our results and the conclusion are found in Sec. V.

II. THEORETICAL MODEL

Horizontally coupled QDs are grown by the depletion of the two-dimensional (2D) electron gas (2DEG) using typically the gated mechanism.[30,31] Such gated QDs have a typical size of about a few tens of nanometers. Consequently, the lowest excitation energy in such a QD system is found of the order of few millielectron volts. When the interdot coupling strength is substantial, the electrons in the coupled dots strongly quantum mechanically couple with each other. As long as the phase is coherent, the electrons can "tunnel" between the adjacent dots, forming different entangled qubits. Using the single-conduction-band effective-mass approximation, which was justified in Ref. 22, the Hamiltonian describing a two-electron coupled-double-QD system containing unintentional charged impurities (charge size Ze) in zero magnetic field reads

$$\widehat{H} = \widehat{h}_1 + \widehat{h}_2 + \widehat{V}_C + \widehat{V}_{\text{e-I}} + \widehat{V}_{\text{I-I}}. \tag{1}$$

Here, the first two terms $\widehat{h}_{i,j}$ are the single-particle Hamiltonian of the two QD electrons (coordinates $\mathbf{r}_i$),

$$\widehat{h}_i = \frac{(i\hbar\nabla_i + e\mathbf{A}_i)^2}{2m^*} + V(\mathbf{r}_i), \tag{2}$$

confined by a potential well $V(\mathbf{r})$. In the present paper, this confining potential is constructed as a linear combination of the three different Gaussians and can be separated into two parts:

$$V(\mathbf{r}) = V_0\left(e^{-[\frac{(x-a)^2}{l_x^2}+\frac{y^2}{l_y^2}]} + e^{-[\frac{(x+a)^2}{l_x^2}+\frac{y^2}{l_y^2}]}\right) + V_b e^{-(\frac{x^2}{l_{bx}^2}+\frac{y^2}{l_{by}^2})}. \tag{3}$$

The first part acts as a double-well confining potential for the coupled-double-dot system and the second part is used to control the electrostatic barrier height between the two dots independently. The set of varying parameters, $V_0, V_b, l_x, l_y, l_{bx}, l_{by}$, characterizes the potential-well depth and barrier height. A nonvanishing overlap between the wave functions of the two QDs signifies the electron virtual tunneling between the two dots, i.e., the exchange energy is nonzero. Because this property can be tuned by the applied gate voltage, this exchange energy thereby can be controlled. It is worth noting that V_b can independently modulate the barrier height, resulting in concomitant change in the interdot separation without modifying the single-particle energy spectrum of the individual QDs in the system.

The last three terms in Eq. (1) are the Coulomb interaction among, respectively, the two electrons

$$\widehat{V}_C = \frac{e^2}{4\pi\epsilon\epsilon_0|\mathbf{r}_{ij}|}, \tag{4}$$

the electron and the impurities

$$V_{\text{e-I}} = \sum_{k=1}^{N_I=2}\sum_{i=1}^{N_e=2}\frac{Z_k e^2}{4\pi\epsilon\epsilon_0|\mathbf{R}_k - \mathbf{r}_i|}, \tag{5}$$

where N_I and N_e denote the number of impurities and electrons, respectively, and the impurities

$$V_{\text{I-I}} = \frac{Z_1 Z_2}{4\pi\epsilon\epsilon_0|\mathbf{R}_1 - \mathbf{R}_2|}. \tag{6}$$

The solution of a single particle confined by a parabolic potential is well known as the Fock–Darwin basis:

$$\varphi_{nl}(\mathbf{r}) = \frac{1}{l_0}\sqrt{\frac{n!}{\pi\,(n+|l|)!}}\left(\frac{r}{l_0}\right)^{|l|} e^{-il\theta} e^{-\frac{r^2}{2l_0^2}} L_n^{|l|}\left(\frac{r^2}{l_0^2}\right), \tag{7}$$

with corresponding energy

$$E_{n,l} = \hbar\omega_0(2n + |l| + 1) \tag{8}$$

where n,l stand for radial and azimuthal quantum numbers, respectively. l_0 is the confinement length which is defined via the confinement frequency ω_0: $l_0 = \sqrt{\frac{\hbar}{m_e^*\omega_0}}$. Using this basis as the radial part, we can construct the many-body wave function for the considered system.

We introduce a dimensionless parameter,

$$\lambda = \frac{l_0}{a_B^*}, \tag{9}$$

where $a_B^* = \frac{4\pi\epsilon_0\epsilon\hbar^2}{m_e^* e^2}$ is the effective Bohr radius, which is used to describe the relation between the effective Rydberg energy $R_y^* = \frac{m^* e^4}{2\hbar^2(4\pi\epsilon_0\epsilon)^2}$ and the confinement energy $\hbar\omega_0$:

$$R_y^* = \hbar\omega_0\frac{\lambda^2}{2}. \tag{10}$$

Both e-e and e-I Coulomb interactions are evaluated in terms of matrix elements as

$$\begin{aligned}\langle\Psi|V_{\text{e-e}}|\Psi\rangle &= V_0^C\langle\Psi|\frac{1}{|\widetilde{\mathbf{r}}_i - \widetilde{\mathbf{r}}_j|}|\Psi\rangle,\\ \langle\Psi|V_{\text{e-I}}|\Psi\rangle &= V_0^C\langle\Psi|\frac{1}{|\widetilde{\mathbf{r}} - \widetilde{\mathbf{R}}|}|\Psi\rangle,\end{aligned} \tag{11}$$

where Ψ denotes the wave function of the system, $\widetilde{\mathbf{r}}_{i,j} = \mathbf{r}/l_0$, $\widetilde{\mathbf{R}} = \mathbf{R}/l_0$, and $V_0^C = e^2/4\pi\epsilon\epsilon_0 l_0$ is the Coulomb energy unit. V_0^C relates to the confinement energy via the relation:

$$V_0^C = \frac{e^2}{4\pi\epsilon\epsilon_0 l_0} = \lambda\hbar\omega_0. \tag{12}$$

The numerical results are implemented for, e.g., a GaAs QD with $m^* = 0.067m_0$, $\epsilon = 13.1$, $g_e = -0.44$, $R_y^* = 5.31$ meV (corresponding to $a_B^* = 10.3$ nm). λ is changed by changing the confinement energy $\hbar\omega_0$. $\lambda = 1$ gives $\hbar\omega_0 = 2R_y^* = 10.62$ meV and corresponding confinement length $l_0 = a_B^* = 10.3$ nm.

For Si/SiGe ($\epsilon = 13$) and Si/SiO_2 ($\epsilon = 6.8$) QDs with a heavier effective mass $m^* = 0.19m_0$, effective Bohr radius and effective Rydberg energy are, respectively, $a_B^* = 4$ nm and $R_y^* = 15$ meV, and $a_B^* = 2.11$ nm and $R_y^* = 44.76$ meV (see, e.g., Ref. 32). $\lambda = 1$ gives $\hbar\omega_0 = 2R_y^* = 30$ meV ($l_0 = 4$ nm) for a Si/SiGe QD and $\hbar\omega_0 = 2R_y^* \approx 90$ meV ($l_0 = 2.11$ nm) for a Si/SiO_2 QD system. Even though our numerical results are applicable to GaAs QD systems, singlet-triplet splitting energies for Si QD systems are also provided in Appendix D for comparison purposes.

Reducing λ means that the effective length l_0 of the QD decreases while the energy spacing $\hbar\omega_0$ between the 2D shells, i.e., the s-, p-, and d-levels, will increase. In the small-λ limit, the problem at hand converts to the problem of independent particles. In the opposite case, very large λ, the problem approaches the classical situation.

In the coupled-double-QD system, the single-particle solutions in each dot are obtained approximately based on an assumption that around the center of the each dot ($\pm a_m$,0) the single-electron problem can be treated as a 2D harmonic oscillator. This means that the confining potential well $V(\mathbf{r})$ performs a quadratic form $V(\mathbf{r}) - E_m \approx \frac{V_0}{l_x^2}[(x \pm a_m)^2 + y^2]$, where E_m is the bottom energy of the potential well, around ($\pm a_m$,0). Changes in E_m when V_b varies can be obtained as the open circles in Fig. 1. The single-particle wave functions now are identical to the Fock–Darwin levels centered at ($\pm a_m$,0)

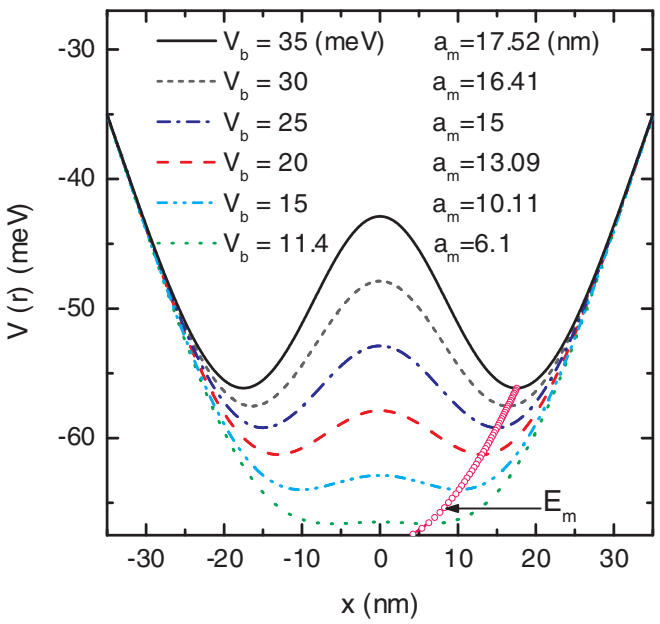

FIG. 1. (Color online) Confinement potential double well of coupled-double QDs modeled along the x direction plotted for different barrier depths V_b (from 35 down to 11.4 meV) (left column). The corresponding double-well minima ($\pm a_m$,0) are indicated in the same line in the right column of the reference. The confinement energy at the two well bottoms E_m is enclosed as the magenta open circles for various values of V_b.

and the single-particle energy spectrum is shifted by an amount of E_m:

$$\varphi_{L(R)}(\mathbf{r}) = \frac{1}{l_0}\sqrt{\frac{n!}{\pi\,(n+|l|)!}}\left(\frac{r_{L(R)}}{l_0}\right)^{|l|} e^{-il\theta} \times e^{-\frac{r_{L(R)}^2}{2l_0^2}} L_n^{|l|}\left(\frac{r_{L(R)}^2}{l_0^2}\right), \tag{13}$$

where $\mathbf{r}_{L,R} = (x \pm a_m, y)$ and $\omega_0 = \sqrt{\frac{2V_0}{m^* l_x^2}}$ is the quadratic confining frequency which defines a new length $l_0^2 = \frac{\hbar}{m^*\omega_0}$, called the confinement length. The single-particle ground-state wave function is

$$\varphi_{L,R} = \frac{1}{\sqrt{\pi} l_0} e^{-\frac{[(x\pm a_m)^2+y^2]}{2l_0^2}}. \tag{14}$$

To quantitatively evaluate the advantage of using the above confining potential present in Eq. (3), we plot in Fig. 1 the confining potential well where its barrier height and the QD centers are modified by changing V_b. Here, V_b is reduced from 35 meV to 30,25,20,15, and 11.4 meV. As a result, the barrier height will decrease, making the electron exchange energy increase. For example, the system with $V_b = 35$ meV has the corresponding $a_m \approx 17.52$ nm ($\approx 1.75 l_0$), and barrier height $\Delta V_b = 13.26$ meV. For $V_b = 30$ meV, these parameters are $a_m \approx 16.41$ nm ($\approx 1.64 l_0$) and $\Delta V_b = 9.65$ meV. Decreasing V_b leads to a shortened interdot separation $2a_m$ and a smaller ΔV_b. Details can be obtained in Fig. 1. In our numerical results, we use $V_b = 30$ meV for most of our calculations except when we examine the barrier height dependence of the exchange energy J where V_b can vary. The center region of each QD, however, has unchanged effective length, namely l_0, regardless of the change in the barrier height. The other parameters taken after Refs. 9,22,23 are $l_x = l_y = 30$ nm, $a = l_{bx} = l_x/2 = 15$ nm, $l_{by} = 80$ nm.

We assume that the impurities are located arbitrarily in or outside the coupled QDs. Their coordinates are $\mathbf{R}_k = (x_k, y_k, z_k)$, $\{\mathrm{k} = 1,2\}$. Theoretically, the effective coupling between electron and localized impurities as well as the coupling between the impurities with each other can be tuned by engineering the impurity charge Z.

Configuration interaction (CI) and molecular orbital (MO) methods are used to numerically solve the Hamiltonian, Eq. (1). Both construct the total wave function of the system as a superposition of different possible quantum configurations (CI) or molecule states (MO) extended in the basis of single-particle wave functions:

$$\Psi(\mathbf{r}_1,\mathbf{r}_2) = \sum_i^{N_c} \psi_i(\mathbf{r}_1,\mathbf{r}_2), \tag{15}$$

where $\psi_i(\mathbf{r}_1,\mathbf{r}_2)$ represents one many-electron configuration as a Slater determinant. Each term of this Slater determinant is a single-electron wave function consisting of the radial part, the Fock–Darwin state $\varphi(\mathbf{r}_1,\mathbf{r}_2)$ defined in Eq. (13), and the electron spin part (detailed justifications are given in Ref. 22).

The singlet-triplet spin splitting energy of the electrons J in such a coupled two-dot system is defined as the energy difference between the two lowest singlet (Ψ^S) and triplet (Ψ^T) states:

$$J = \langle\Psi^T|\widehat{H}|\Psi^T\rangle - \langle\Psi^S|\widehat{H}|\Psi^S\rangle. \tag{16}$$

A. Hund–Mulliken

In the Hund–Mulliken model, the energy spectrum consists of four levels which are four possible superpositions of the: four basis (three singlets and one triplet) wave functions:

$$\begin{aligned}
\psi_1^S(\mathbf{r}_1,\mathbf{r}_2) &= \frac{1}{\sqrt{2}}[\varphi_L(\mathbf{r}_1)\varphi_R(\mathbf{r}_2) + \varphi_L(\mathbf{r}_1)\varphi_R(\mathbf{r}_2)],\\
\psi_2^S(\mathbf{r}_1,\mathbf{r}_2) &= \varphi_L(\mathbf{r}_1)\varphi_L(\mathbf{r}_2),\\
\psi_3^S(\mathbf{r}_1,\mathbf{r}_2) &= \varphi_R(\mathbf{r}_1)\varphi_R(\mathbf{r}_2),\\
\psi^T(\mathbf{r}_1,\mathbf{r}_2) &= \frac{1}{\sqrt{2}}[\varphi_L(\mathbf{r}_1)\varphi_R(\mathbf{r}_2) - \varphi_L(\mathbf{r}_1)\varphi_R(\mathbf{r}_2)].
\end{aligned} \tag{17}$$

In the coupled-QD system without an impurity, these three singlets do not couple with the maximally entangled triplet state ψ^T; therefore they can be treated separately. The entire Hamiltonian matrix represents these singlets and triplets as independent blocks.

B. Configuration interaction

The most difficult task in finding the eigenvalues of a coupled two-dot system lies in the basis choice among which the Fock–Darwin basis and the Gaussian basis are the most widely used. However, in both cases a closed analytical form for the Hamiltonian matrix elements, essentially the e-e Coulomb matrix elements, has not yet been obtained. The reason is that the single-particle solutions of different dots i) have distinct zero points shifted to the two bottoms of the confining potential well and ii) thus are not orthogonal with each other. Consequently, the number of distinguishable single-particle quantum states for the double-dot system will be doubled. Effectively, the size of the entire Hamiltonian increases in comparison with the single-dot case. Quantitatively, for $S_z = 0$ subspace, such a number is four times larger than that of the single-dot problem ($2N \times 2N$). Specifically, if only the s-waves are taken into account, the number of configurations in the subspace $S_z = 0$ is 1 for single-QD and 4 for coupled-two-dot systems and if the s- and p-waves are included, those numbers are 9 and 36, respectively.

The above fact poses much difficulty for solving the eigenvalues of the coupled-QD Hamiltonian. The most time-consuming part is spent in calculating the Coulomb matrix elements. In the problem at hand, the number of Coulomb elements increases due to the e-I exchange interaction. However, from the following facts, one can take out nonphysical excited single-particle quantum states: i) the form of the confining potential, which is tuned electrostatically by metal top gates, is not exactly known, and ii) the barrier potential height is finite. The latter factor validates the harmonic approximation for the confinement potential double well, resulting in only a limited number of Fock–Darwin states involved.

III. IMPURITY EFFECTS IN SINGLE QUANTUM DOTS

In the single-QD case, we assume that there is only one impurity and the impurity is located along the z axis, i.e., $R = (0,0,d)$. The addition Coulomb interaction of the electrons with the impurity is obtained analytically (see Appendix A):

$$V_{n_1 l_1}^{n_2 l_2}(\widetilde{R}) = \delta_{l1,l2}\frac{2}{\sqrt{\pi}}\frac{\Gamma(n_1+l^+ +1)\Gamma(n_2+l^+ +1)}{\sqrt{n_1!n_2!(n_1+l^+)!(n_2+l^+ +1)!}}\sum_{j=0}^{n_1}\sum_{k=0}^{n_2} \times \frac{(-n_1)_j(-n_2)_k\Gamma(l^+ +j+k+1)\Gamma(l^+ +1)}{j!k!\Gamma(l^+ +j+1)\Gamma(l^+ +k+1)} I_m(\widetilde{R}), \tag{18}$$

where $l^+ = |l_1| = |l_2|$ and

$$I_m(\widetilde{R}) = \int_0^\infty \frac{e^{-\widetilde{R}^2 u^2}}{(1+u^2)^{m+1}} du. \tag{19}$$

Integral (19) can be obtained through the recurrences

$$I_0(\widetilde{R}) = \frac{\pi}{2} e^{\widetilde{R}^2}\mathrm{erfc}(\widetilde{R}),$$
$$I_1(\widetilde{R}) = \frac{1}{2}[(1-2\widetilde{R}^2)I_0\widetilde{R} + \sqrt{\pi}\widetilde{R}], \tag{20}$$
$$I_m(\widetilde{R}) = \left(-\frac{\widetilde{R}^2}{m} + 1 - \frac{1}{2m}\right) I_{m-1}(\widetilde{R}) + \frac{\widetilde{R}^2}{m} I_{m-2}(\widetilde{R}),$$

where $\mathrm{erfc}(x)$ is the complementary error function,

$$\mathrm{erfc}(x) = \int_x^\infty \frac{e^{-x^2 t^2}}{1+t^2} dt, \tag{21}$$

which rapidly decreases in x. $(x)_n = x(x+1)(x+2)...(x+n-1)$ is the Pochhammer function. Several values of the complementary error function which can be obtained in any numerical library are $\mathrm{erfc}(0) = 1$, $\mathrm{erfc}(0.01) \approx 0.98872$, $\mathrm{erfc}(0.1) \approx 0.88754$, $\mathrm{erfc}(0.5) \approx 0.47950$, $\mathrm{erfc}(1) \approx 0.1573$, $\mathrm{erfc}(2) \approx 0.00468$, etc.

A. Perturbative and exact calculations

Following the e-I interaction whose matrix elements are expressed in Eq. (18), there is mixture between different states with different total radial quantum numbers. Consequently, the ground-state wave function, e.g., for the $N_e = 1$ electron, is no longer the only one s $(n = 0, l = 0)$ quantum state. Instead, it consists of several quantum states whose contributions C_i are different:

$$\Psi = \sum_{i=1} C_i \psi_i. \tag{22}$$

For $N_e = 2$ electrons without impurity, increasing λ results in the ground-state mixing of different configurations. The two electrons will occupy higher Fock–Darwin states with decreasing energy spacing to lower their Coulomb repulsion. The easiest way to check the accuracy of the numerical results when the impurity is present is to consider the limitation when weak perturbation works perfectly. The first-order perturbation approximation

$$E = E_0 + Z\sum_{i=1}^{N_e}\langle\Psi_0|V(|\mathbf{r}_i - \mathbf{R}|)|\Psi_0\rangle + O(Z^2), \tag{23}$$

where E_0 is the ground-state energy of the QD, and the ground-state wave function Ψ_0 in the case without impurity is a good one when $Z < 1$. For the sake of simplicity in evaluating the perturbative part in Eq. (23) for both $N_e = 1$ and 2 electrons, we assume that Ψ_0 in the case $Z = 0$ is a single term: the s-state. For $N_e = 1$ electron, this is always satisfied and its radial part is

$$\Psi_0(r) = \frac{1}{l_0\sqrt{\pi}} e^{-\frac{r^2}{2l_0^2}}. \tag{24}$$

The situation changes for $N_e = 2$. The above condition for Ψ_0 to be a single term is satisfied only when $\lambda < 1$. If so, the two electrons obeying the Pauli exclusion principle with spins antiparallel will mainly stay in the s-orbital in case no impurity is present because their Coulomb repulsion is small compared with the confining energy. The ground-state wave function is

$$|\Psi_0\rangle = c_{s\uparrow}^\dagger c_{s\downarrow}^\dagger |0\rangle. \tag{25}$$

Using this assumption, the total energy is estimated theoretically for the single-electron QD,

$$E_{(N_e=1)} = E_{0_{(N_e=1)}} + 2\sqrt{\pi}Z\lambda\hbar\omega_0 e^{\widetilde{R}^2}\mathrm{erfc}(\widetilde{R}) + O(Z^2), \tag{26}$$

and the two-electron QD,

$$E_{(N_e=2)} = E_{0_{(N_e=2)}} + 4\sqrt{\pi}Z\lambda\hbar\omega_0 e^{\widetilde{R}^2}\mathrm{erfc}(\widetilde{R}) + O(Z^2). \tag{27}$$

We plotted in Fig. 2 the energy shift due to the presence of the impurity as a function of d using the above theoretical estimations (red dash-dotted curve) and the numerical results (black solid curve) for $Z = 0.1$ and $\lambda = 0.1$ ($l_0 = 1.03$ nm and $\hbar\omega_0 = 200R_y^* = 1.062$ eV) for $N_e = 1$ (upper curves) and 2 (lower curves) electrons. Both theoretical and numerical results are in good agreement.

A small comment is made in case d is large. As seen from Fig. 2, the e-I interaction goes to zero slowly when d increases to a relatively large value, say $d > a_B^*$. The answer lies in the product $[e^{\widetilde{R}^2}\mathrm{erfc}(\widetilde{R})]$, where the exponential function increases in d competitively with the complementary error function which decreases in d.

The first-order perturbation theory works very well as long as $Z < 1$ and λ is small enough; if λ increases, different e-I couplings of different configurations will occur which result in the presence of a substantial number of nonzero off-diagonal terms. This fact leads to an increasing difference between the first-order calculations and the numerical results. For example, in the two-electron QD as plotted in the inset of Fig. 2, this difference for $\widetilde{R} = 0$, which is also the largest value, is about 6% when λ increases to 0.5. This 6% come from the configurations with minor contributions $(n_1 = 1, l_1 = 0; n_2 = 1, l_2 = 0), (0,1;0,-1)$, etc. n_1, l_1 and n_2, l_2 are the radial and azimuthal quantum numbers of the two electrons.

Practically, one often has GaAs QDs with $\lambda > 1$, i.e., larger QDs need to be considered. To describe such QDs, numerical

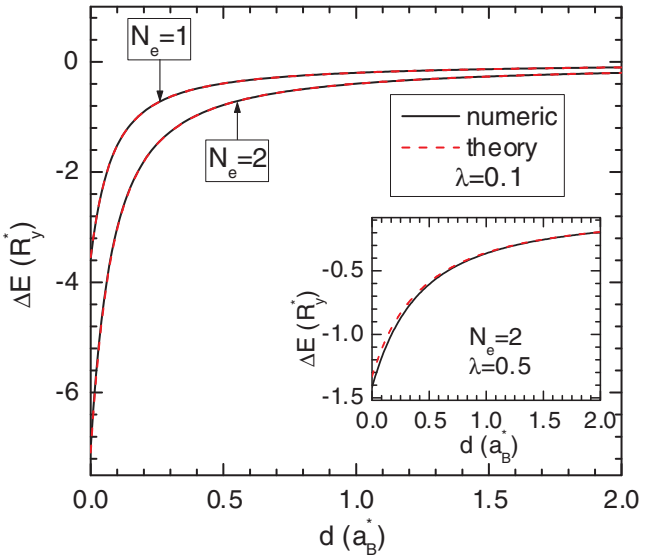

FIG. 2. (Color online) Agreement between theoretically perturbative (red dash-dotted curve) and exact diagonalization (black solid curve) calculations in the shift of the ground-state energy due to the presence of the impurity in single-electron (two upper curves) and two-electron (two lower curves) QDs for $\lambda = 0.1$. The impurity effective charge is $Z = -0.1$. The inset shows additional data for the case in which λ is increased to 0.5 to examine whether the perturbative calculations hold reliably. This energy shift is identical to the binding energy of the system and scaled to the Rydberg energy $R_y^* = 5.31$ meV for GaAs QDs.

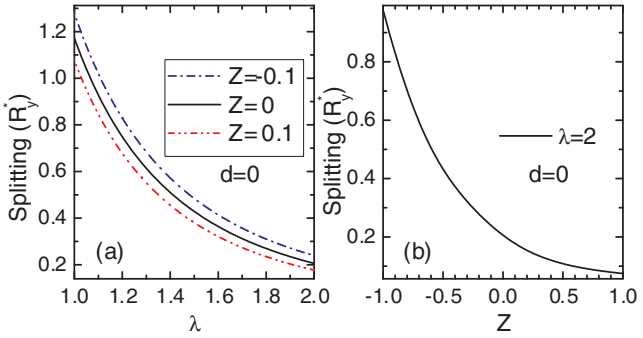

FIG. 3. (Color online) Splitting energy of the two lowest singlet and triplet energy levels as a function of (a) Coulomb interaction strength λ for three different $Z = -0.1$ (blue dashed-dotted curve), 0 (black solid curve), and 0.1 (dash-dotted-dotted curve) and (b) impurity effective charge Z within the range $(-1,1)$ for the case $\lambda = 2$. The impurity is located at the origin of the single two-electron QD: $d = 0$.

calculations are used for different values of λ. Here, we examine the case of $\lambda = 2$ which has $l_0 = 2a_B^* = 20.6$ nm and the corresponding $\hbar\omega_0 = R_y^*/2 = 2.655$ meV. The Coulomb interaction unit ($V_0^C = 5.31$ meV) in such a QD system is (two times) larger than the confining energy $\hbar\omega_0$.

B. Singlet-triplet splitting energy

The Coulomb interaction between the QD electrons strongly competes with the confining energy and with the e-I interaction as Z and/or λ increase. Increasing λ means that the confining energy becomes smaller with respect to the Coulomb interaction. As a result, electrons start to occupy higher Fock–Darwin levels. At zero B field and in the absence of impurity, the ground state consists of several Fock–Darwin states where the dominant component is the s-wave term. In the presence of a charged impurity, those electron configurations that fulfill $L =$ const form different L subgroups with nonzero contributions to the total wave function of the system. Increasing the effective charge Z results in a strong mixing between those subgroups. Consequently, there are more than one states which play as dominant components to the total wave function. We plot in Figs. 3(a) and 3(b), respectively, the splitting energy between the ground state (singlet) and the first excited state (triplet) as a function of λ and Z in case the impurity is located at the center of the single QD. As λ increases [see Fig. 3(a)], the splitting becomes smaller for both with- and without-impurity cases. It is because the singlet and the triplet states have many similar nonzero configurations. Details are found below from the discussion for particular values of Z. From Fig. 3(a) we also notice that the energy splitting shift due to the presence of the impurity remains almost unchanged by changing λ for both cases $Z = -0.1$ (blue dashed dotted curve) and $Z = 0.1$ (red dash-dotted-dotted curve). It is because the impurity location is examined at the center of the QD, $d = 0$. Such a splitting shift will change if the impurity is displaced to any other off-center position, $d \neq 0$.

The Z dependence of the splitting energy in Fig. 3(b) for $\lambda = 2$ shows a continuous decrease as Z changes its sign from negative $(-1,0)$ to positive $(0,1)$. The decrease is significant around $Z = -1$ which coincides with the physics discussed above for the negative $Z = -0.1$ and -1 cases.

It is found that for $Z = -0.1$ and -1 the ground state and the first-excited state in the two-electron QD containing a single charged impurity are the singlet and the triplet, respectively. Their major components are, respectively, the s-s and the s-p configurations, i.e., one electron is in the s- and the other in the s-(p-)orbital. Note that the s-s overlap has only one maximum at the origin. In the opposite case, the s-p overlap exhibits a minimum at the origin.

With changing the position of the impurity, the energy spin splitting of the singlet-triplet states is obtained in Fig. 4(a) for $Z = -0.1$ and Fig. 4(b) for $Z = -1$. The presence of the impurity results in an increase in the splitting which is largest when the impurity is located at the center of the dot [as illustrated in Figs. 4(a) and 4(b) for $Z = 0$ (dot lines) and for $Z < 0$ (solid lines)].

The magnitude of the splitting over an impurity charge unit $[(E_1^I - E_0^I) \equiv$ splitting$]$/Z, where $E_{0,1}^I$ is the energy of the ground state and the first-excited state in the doped QD, is found smaller for the larger-Z case [see Figs. 4(a) and 4(b)] for a certain d value. This means that the e-I attraction becomes dominant over the e-e Coulomb interaction. As a result, each state consists of different configurations with compatible contributions to the total wave function. For example, by increasing the e-I effective strength from $Z = -0.1$ [Fig. 4(a)] to $Z = -1$ [Fig. 4(b)], the contribution of the singlet s-configuration decreases from $C_0^2 \approx 0.83$ to respectively $C_0^2 \approx 0.64$. The compensatory parts come from other configurations which also have $L = 0$ such as $(n_1 =$

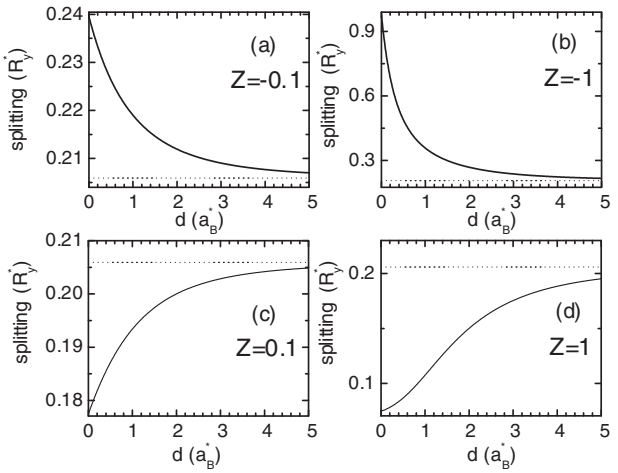

FIG. 4. Splitting of the two lowest singlet and triplet states as a function of the impurity position in a two-electron single QD for four different effective charges of the impurity; (a) $Z = -0.1$, (b) -1, (c) 0.1, and (d) 1 in case $\lambda = 2$ ($\hbar\omega_0 = 2R_y^*/4 = 2.655$ meV). Dotted lines are the data obtained for the zero-effective-charge case ($Z = 0$) for reference.

$0,l_1 = 0; n_2 = 1, l_2 = 0$), (0,0;2,0), (0,0;3,0), etc. Those states stay closer in energy with increasing λ (=2 in this case).

Above we discussed the impurity effect for an attractive impurity (positively charged $Z < 0$). A negatively charged impurity which induces a repulsive coupling with electron is examined in Figs. 4(c) and 4(d) for two effective charges, $Z = 0.1$ and $Z = 1$. The splitting energy between the ground-state singlet and the first-excited triplet is plotted as a function of the impurity position d. Apparently, when the impurity is found at the origin $d = 0$, it repels the two electrons most. The probability of the electrons to be found at the origin (s-orbital) reduces significantly. In this case, the electrons can be found at other higher Fock–Darwin states. This means that the ground-state energy becomes closer in energy to the first-excited state. That explains a smaller splitting energy we obtain for $Z = 0.1$ [see Fig. 4(c)] and $Z = 1$ [see Fig. 4(d)] as compared with, respectively, the cases $Z = -0.1$ [see Fig. 4(a)] and Z $= -1$ [see Fig. 4(b)]. Moreover, we see from Figs. 4(c) and 4(d) that when the impurity is moved away from the center of the QD, the splitting energy starts to increase. In other words, the probability of finding the electrons in the s-orbital increases.

C. Impurity effect on the energy spectrum

Technically, the presence of a charged impurity leads to an increase in the number of nonzero off-diagonal elements of the Hamiltonian matrix. We present such examination on the energy spectrum of the two-electron single QD as a function of the impurity position. The competition between the two types of Coulomb interaction results in different relative orders of the energy levels depending on both the impurity charge Z and the impurity position d.

For the weak-perturbation case, $Z = -0.1$ [Fig. 5(a)], the e-I interaction strength is much smaller (10 times) than the e-e interaction. The ground-state energy (level's degeneracy $g = 1$) is the singlet state where the configuration with the

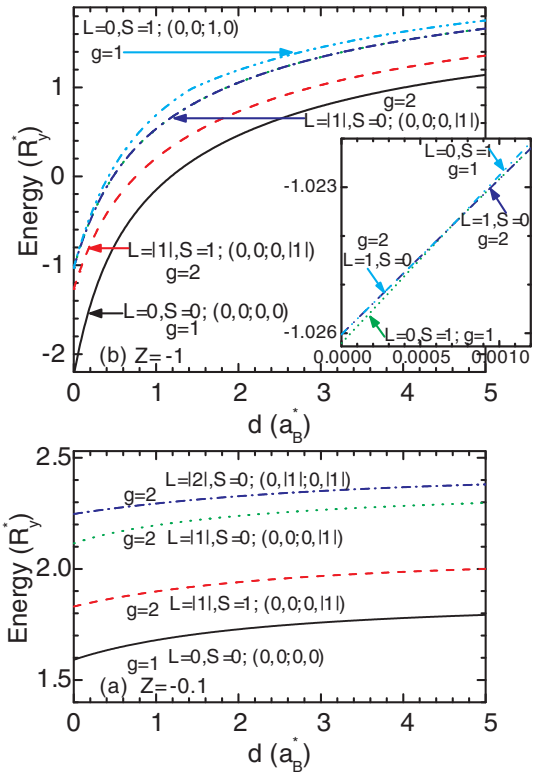

FIG. 5. (Color online) Low-level energy spectrum as a function of d of a two-electron QD in case (a) $Z = -0.1$ and (b) $Z = -1$ for $\lambda = 2$. Each level is labeled by g as the level's degeneracy, L, S as total angular momentum and total spin, and the major electron configurations (n_1,l_1,n_2,l_2). n_1,l_1 and n_2,l_2 are the radial and azimuthal quantum numbers for electron, 1 and 2. The inset in (a) is a magnification of the main plot which highlights the region with the occurrence of the crossing at $d/a_B^* \approx 0.0008$.

two electrons in the s-orbital is highly dominant. The first- and second-excited states have degeneracies $g = 2$ due to the symmetry of $L = \pm 1$ states. Note that at $B = 0$ the results are independent of spins. We present the results in the $S_z = 0$ subspace. We discuss the $L = 1$ case. In the first-excited state, the most dominant configuration is (0,0;0,1), the second configuration is (0,$-$1;0,2), and the last configuration is (0,0;1,1). These three configurations and their exchange states have coefficients with opposite signs in the wave function ($C_{(0,0;0,1)} = -C_{(0,1;0,0)} \approx 0.7$, $C_{(0,-1;0,2)} = -C_{(0,2;0,-1)} \approx 0.07$, and the other $C_{(1,1;0,0)} = -C_{(1,1;0,0)} \approx 0.06$), leading to the triplet first-excited state. The second-excited state has an opposite manner leading to the total spin $S = 0$. Plus, the second dominant configuration and the third dominant configuration in the second-excited state switch their relative orders (sorted in probability) in the total wave function as compared with their orders in the first-excited state. The highest energies in Fig. 5 are the ($L = \pm 2$, $S = 0$) states with the largest configuration (0, ± 1; 0, ± 1). Other considerable configurations are (0,0; 0, ± 2) and (0, $\mp$ 1; 0, ± 3).

In the two energy spectra presented in Fig. 5, the ground state and the first-excited state remain as singlet and triplet states. The fourth, fifth, and the sixth levels, which are the ($L = 0$, $S = 0$) and ($L = \pm 1$,$S = 0$) states, exhibit a crossing at $d = 0.0008a_B^*$. For $d < 0.0008a_B^*$, the ($L = 0$, $S = 1$) state

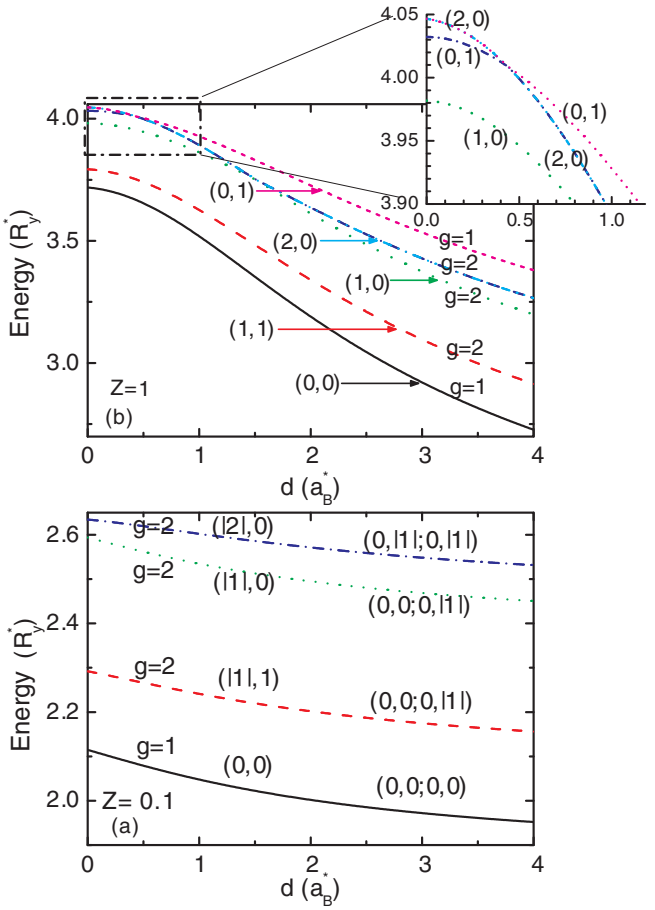

FIG. 6. (Color online) Low-level energy spectrum of two-electron single QD containing a repulsive impurity (a) $Z = 0.1$ and (b) 1 for $\lambda = 2$. The inset in (a) is the magnification of the main plot into the region $d = 0{,}1.1a_B^*$) to signify the crossing at $d = 0.44a_B^*$ between the states (L = 0, S = 1) and (L = 2, S = 0).

has a lower energy than the two-fold degenerate ($L = \pm 1$, $S = 0$) state. The major contributions to the wave function of the lower energy are, sorted in probability, (0,0; 1,0), (0,0; 2,0), and (0,0; 3,0). Increasing $d \geqslant 0.0008a_B^*$ leads to the exchange between the ($L = 0$, $S = 1$) and ($L = \pm 1$, $S = 0$) states where the two-fold degenerate ($L = \pm 1$, $S = 0$) state has lower energy.

The above physics resulted from the dominant e-I interaction when $Z = -1$. The ($L = 0$, $S = 1$) and ($L = 1$, $S = 0$) states now have smaller energies than the ($L = 2$, $S = 0$) state. Besides, it is found that the two-fold degenerate states (0, $\pm$1,0, $\mp$1), which dominate in the third-excited energy level ($L = 0$, $S = 1$) for $Z = 0$, have higher energies when the impurity is present.

The positive-Z case does not affect the energy spectrum as strongly as does for the negative-Z case. The reason is that the impurity in the positive-Z case induces the same type of Coulomb interaction with the QD e-e interaction. However, such an exchange in the relative order of the energy levels, e.g., between the ($L = 0$,$S = 1$) and (2,0) states (corresponding to levels 4−6) can still be observed (see the crossing at $d = 0.44a_B^*$ in Fig. 6). The point $d = 1.52a_B^*$ appears as a crossing-like point but it is only an almost-zero energy gap between the (1,0) and (0,1) states. Similar to the attractive impurity case, a larger e-I interaction also results in a smaller energy gap between the first-excited state and the second-excited state.

D. Summary for the impurity effect on the energy spectrum of two-electron single QDs

The cases of negative and positive Z affect the energy spectrum in different manners. Apparently, the impurity effect for the $Z < 0$ case is expected to be stronger than the $Z > 0$ case. When $Z = -1$ the e-I interaction strongly competes and dominates over the e-e interaction. Let us take an example to illustrate the point. In the weak-perturbation regime, i.e., $|Z| = 0.1$, the e-e interaction dominates over the e-I interaction. The order of the low-level energy spectrum then exhibits no difference between those two cases, $Z = \pm 0.1$. Now, $|Z|$ is increased to 1. However, the system with negative Z exhibits a stronger e-I interaction. Such a strong effect for the attractive case $Z = -1$ is observed in the exchange of the singlet and triplet states with $L = 1$ and $L = 0$ as seen in the inset of Fig. 5(b). For the repulsive case $Z = 1$, this exchange is no longer observed. Only the exchange between the triplet $L = 0$ and singlet $L = 2$ is found. The repulsive e-I interaction in

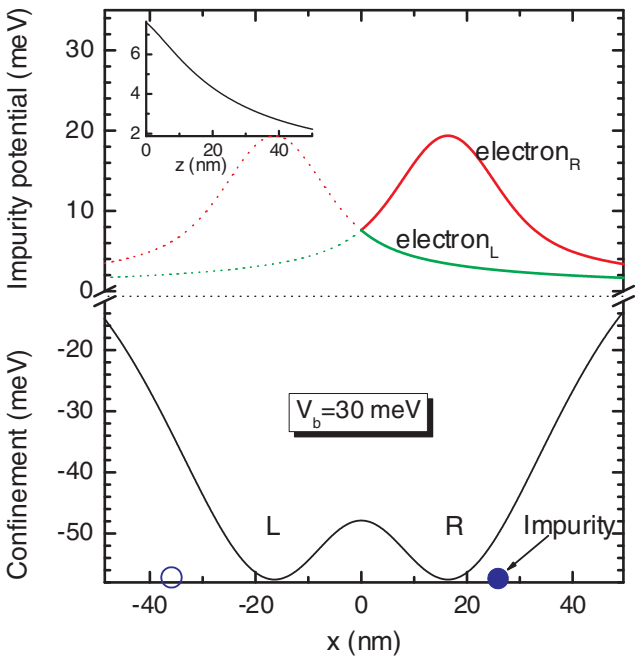

FIG. 7. (Color online) Schematic plot of the confining potential (bottom) and the charged impurity potential (top) in a coupled-two-dot system. We assume the impurity is negatively charged with $Z_1 = 1$ and is located along the line connecting the two double-well minima ($\pm a_m$) where $\pm$, respectively, indicates the left (L) and the right (R)-dot. The two solid lines on top depict the impurity potential on the two individual electrons in the two separate QDs. The upper solid line is the potential of the electron in the right dots and the lower solid line of the electron in the left dot, respectively. Dotted lines on top depict the other case when the impurity is located on the other half of the x axis ($x_1 < 0$), i.e., it can be found inside the left dot. V_b is taken to be 30 meV. The inset is the Coulombic potential of the impurity, located along the growth direction, which equally repels the two separate QD electrons.

the case $Z = 1$ is manifested in the presence of the ($L = 2$, $S = 0$) state which was not seen in the lowest energy levels shown in Fig. 5(b) for $Z = -1$.

IV. COUPLED QUANTUM DOTS

Numerical results for the singlet-dot case were discussed in detail, mostly for $\lambda = 2$ corresponding to $l_0 = 2a_B^* = 20.6$ nm. This value of λ was studied based on the realistic sizes of GaAs single QDs. However, we also theoretically discussed the results for a typical range of $\lambda = (1,2)$ as seen in Fig. 3(a). For the coupled-QD problem, we used the optimized parameter set after Ref. 22 where $l_0 = 10.01$ nm ($\hbar\omega_0 = 11.24$ meV). Mapped on the single-dot case, the coupled-two-dot system will have "λ" ≈ 1. The model of coupled dot system in the presence of a charged impurity can be schematically described in Fig. 7. We plotted the impurity potential in the top panel for the case in which the impurity is located along the line connecting the two minima of the double well and in the inset for the case along the growth direction. It is clear that the impurity effect is largest when the impurity is at either of the two minima of the confining potential well in the former case, whereas the latter case has the largest impurity effect when the impurity is found at the center of the system, i.e., $R = 0$. We label the two impurity coordinates as $\mathbf{R}_{1(2)} = (x_{1(2)}, y_{1(2)}, z_{1(2)})$.

A. Singlet-triplet splitting

1. Impurity-position dependence

In the coupled QD system without impurity and without magnetic field ($B = 0$), the two lowest energy levels are the maximally entangled exchange spin states, respectively, the singlet Ψ_1^S and the triplet Ψ^T. The next higher excited states are the linear combination of the two doubly occupied singlets which result in "bonding" ($\frac{\psi_2^S + \psi_3^S}{\sqrt{2}}$) and "antibonding" ($\frac{\psi_2^S - \psi_3^S}{\sqrt{2}}$) states.

Let us first consider the simplest case, when the system contains only a single charged impurity $\mathbf{R}_1 = (x_1, y_1, z_1)$ (effective charge Z_1) and the impurity plays only as a weak perturbation to the coupled-dot system. However, there will be no restrictions to the impurity location in or outside the system. Such a system allows us to provide a direct comparison with the single-dot case discussed earlier.

In the case in which the e-I interaction is attractive coupling, i.e., $Z_1 < 0$, the singlet-triplet exchange energy J is shown in Fig. 8(a). When the impurity is located along the z axis [see the black solid curve in Fig. 8(a)], the presence of the impurity increases the singlet-triplet spin splitting J between the two electrons as compared with the case when no impurity is present [see horizontal gray dotted curve in Fig. 8(a)]. This is understood as both electrons are attracted toward the impurity. Because the impurity equally couples to the electrons, the system favors the antiparallel electron spin state. This type of e-I coupling reduces the total energy of the system [negative binding energy presented as black solid curve in Fig. 8(c)]. As the impurity is moved away from the origin [$z_1 \neq 0$ – still the black solid curve in Fig. 8(a)], J will decrease. Such a decrease can be evaluated via Eq. (A4) (see Appendix A) as the product of an exponential and complementary error function.

When the impurity is located along the z direction of either the two separate dots, e.g., of the right dot i.e. $\mathbf{R}_1 = (a_m, 0, z_1)$ [see red dashed curve in Fig. 8(a)], J remains larger than the J for the case in which without impurity, $Z_1 = 0$. However, J

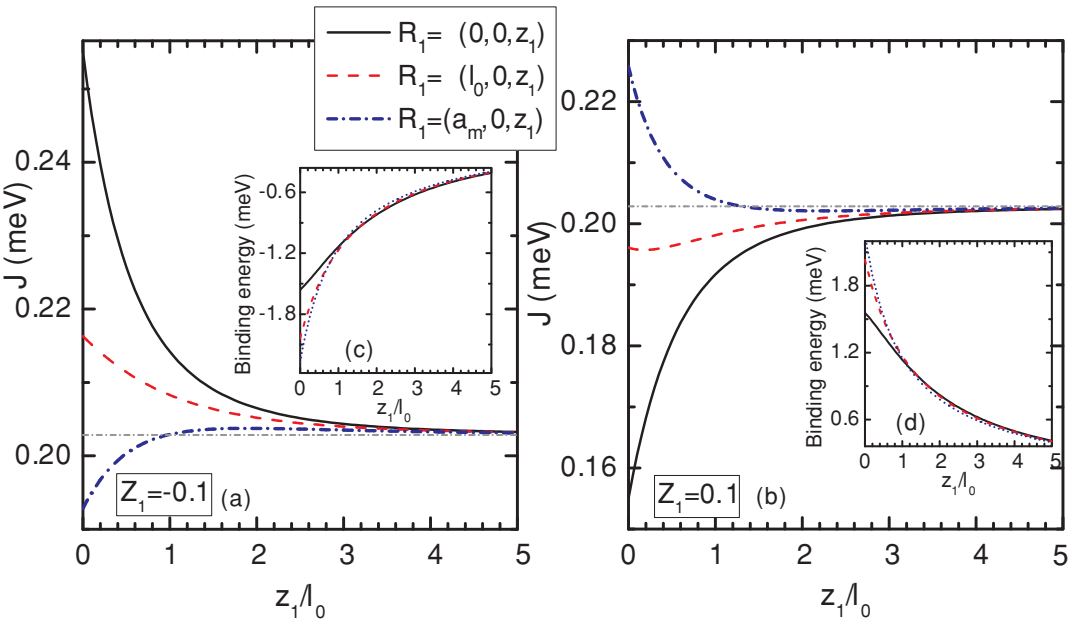

FIG. 8. (Color online) Singlet-triplet splitting energy calculated as a function of z_1 coordinate of a single impurity in the case $Z_1 = -0.1$ [(a) and (c)] and $Z_1 = 0.1$ [(b) and (d)] for three different positions of the impurity x coordinate, $x_1 = 0$ (black solid curve), $x_1 = l_0$ (red dashed curve), and $x_1 = a_m$, either of the two double-well minima (blue dashed-dotted curve). V_b is taken to be 30 meV. For comparison purposes, we recall the value of $J \approx 0.204$ meV as the horizontal dashed-dotted line in the case when no impurity is present for $B = 0$. Insets (c) and (d) show the corresponding total binding energy of the three cases plotted in each main plot (a) and (b).

behaves very differently from the above two cases, $x_1 = 0$ and $x_1 = l_0$. The impurity not only no longer attracts equally the two-QD electrons (similar to the $x_1 = l_0$ case) but also affects the doubly occupied states most. J in this case intersects the splitting energy of the $Z_1 = 0$ case at $z_1 \approx l_0$. Close to the QD sample, i.e., $z_1 \ll l_0$, J is always smaller than the splitting energy for the without-impurity case, about 10%. We reserve the detailed physical discussion around $(\pm a_m,0)$ for a later discussion when we examine the case for the impurity located along the x axis.

We expect that a repulsive impurity induces an opposite spin order of the two-electron spin orientations: the parallel spin state. This is illustrated in Fig. 8(b). A weakly repulsive impurity ($Z_1 = 0.1$), located along the z axis (black solid curve), has the smallest exchange energy (≈ 0.17 meV) when it is, apparently, at the origin: $z_1 = 0$. The reason is the impurity now repels both electrons. The e-I addition energy lifts up, by approximately a few millielectron volts, the total energy of the coupled-two-dot system [see the positive binding energy presented in Fig. 8(d)]. J rapidly increases and reaches the value of the nonimpurity case as the impurity is engineered relatively far from the origin, say $3l_0$.

The ground state consists of all three Hund–Mulliken singlets, i.e., the total wave function $\Psi_{GS} = \{\psi_1^S, \psi_2^S, \psi_3^S\}$. However, two doubly occupied states play a small part, which are $\approx 2\%$, to the total wave function.

The binding energy of the impurity, which is defined as the energy difference of the system with and without a charged impurity, shown in Figs. 8(c) and 8(d), was partially discussed above. In both cases $Z_1 = \mp 0.1$, around $z_1 = 0$, the absolute value of the binding energy is found largest in the case in which the impurity is placed closer to either of the two minima of the well ($x_1 = a_m$): 2.2 meV compared with 2 meV and 1.53 meV of the $x_1 = l_0$ and $x_1 = 0$ cases, respectively. Beyond a critical z_1, say $z_1 > 2l_0$, the most dominant binding energy case ($x_1 = a_m$, black solid curve) becomes less dominant and compatible with the other cases, $x_1 = 0$ and l_0. All three curves in Figs. 8(c) and 8(d) convert to the situation without impurity at the large-z_1 limit.

Now, we consider the case when the impurity is found inside the QD. In particular, we discuss the impurity effect when the impurity is found on the x or y axis, along which the confining potential is constructed.

Because the $Z_1 = \mp 0.1$ case was found to weakly affect the QD qubits and that the doubly occupied states have very small contributions to the singlet-triplet splitting, we can now use Heitler–London model to analytically check our numerical results. We found qualitative agreement between the results presented in, e.g., Fig. 9 and the analytical results shown in Eq. (B1), in particular the minimum (maximum) in J for $Z = -0.1$ (0.1). Details are collected in Appendix B.

As signified in the top plot in Fig. 1, the absolute value of the effective e-I coupling exhibits a maximum at the either of the two well minima and decreases rapidly as the impurity position is out of the minima [analytical matrix elements are presented in Eq. (A5) in Appendix A]. However, the overlap between the two coupled QDs has a maximum at the origin (see, e.g., Ref. 23). In the weak impurity perturbation, i.e., $Z_1 \ll 1$, these two terms compete with each other. As a result, the singlet-triplet spin splitting J for $Z_1 = -0.1$ has the impurity position dependence as shown in Fig. 9. J has a maximum at the origin where the overlap between the two coupled dots is largest, and

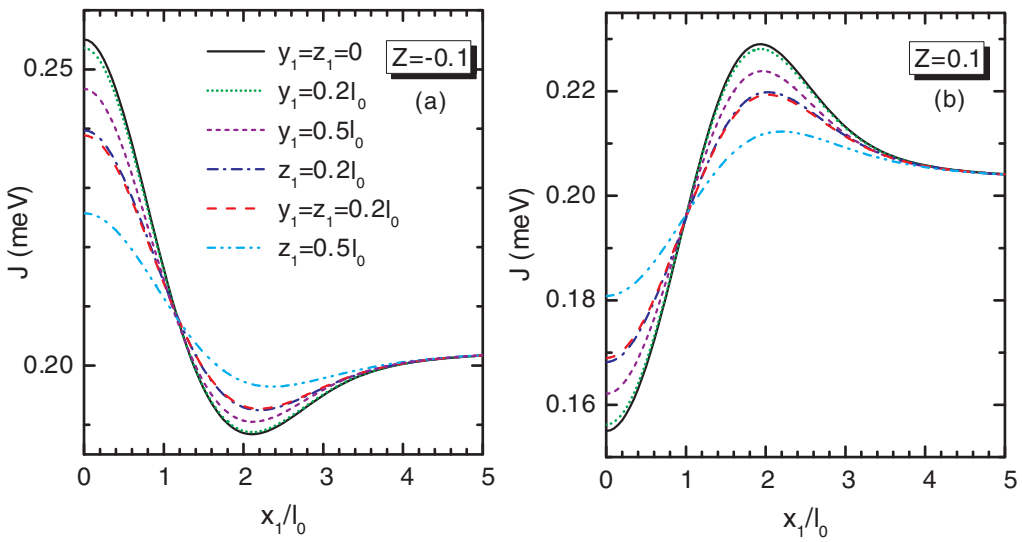

FIG. 9. (Color online) Singlet-triplet splitting energy as a function of the x coordinate of the impurity position for (a) $Z_1 = -0.1$ and (b) $Z_1 = 0.1$ for $V_b = 30$ meV. The y and z coordinates of the impurity position, R_y and R_z, are varied from the origin (black solid curve) to $R_y = 0.2l_0$ (green dotted curve), $R_y = 0.5l_0$ (violet short-dashed curve), $R_z = 0.2l_0$ (blue dash-dotted curve), $R_y = 0.2l_0, R_z = 0.2l_0$ (red dashed curve), and $R_z = 0.5l_0$ (dash-dotted-dotted curve). The omitted coordinates are implied to be 0. We cover many different possible positions of the impurity such that it can be along the x axis or along the y axis, or around the either the two minima with both x_1 and y_1 coordinates slightly changed while $z_1 = 0$, etc. Notice the case where the impurity is shifted along the y axis. This shift does not add much physics to the system. For example, see the insubstantial difference between the exchange energies in the black solid curve ($y_1 = x_1 = 0$) and green dotted ($y_1 = 0.2l_0$) curve, or between the blue dashed-dotted ($z_1 = 0.2l_0$) and red dashed ($y_1 = z_1 = 0.2l_0$) curves, etc, presented in both (a) and (b).

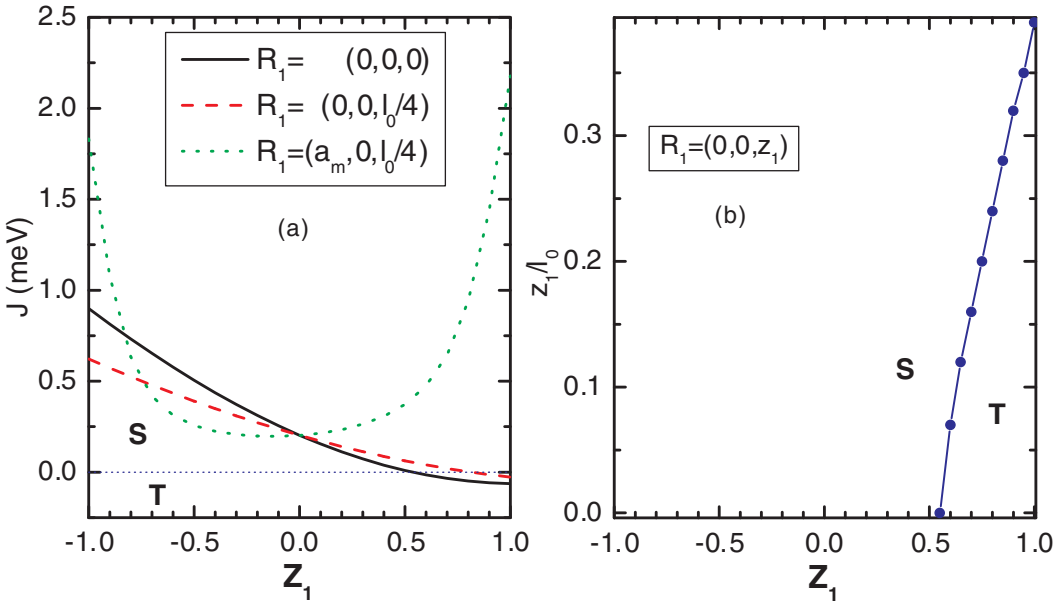

FIG. 10. (Color online) (a) Singlet-triplet spin splitting J as a function of the impurity effective charge Z_1 within the range $Z_1 = (-1,1)$ for three different positions of the impurity along the z axis and (b) the singlet-triplet state diagram as a function of the impurity charge Z_1 and its position along the z axis. V_b=30 meV. S and T refer, respectively, to the singlet and triplet state. When the impurity is positioned close to the origin [$z_1 = 0$ (black solid curve) and $z_1 = 0.25l_0$ (red dashed curve) in (a)], the system exhibits a triplet-singlet transition at $Z_1 = 0.54$ and 0.8, respectively. The green dotted curve is added for reference purposes which shows that as the impurity is found at (or close) to either the left or right minimum of the well, the system is always the singlet.

the binding energy exhibits a maximum around $x_1 = 1.6l_0$ which is identical to the quasi-bottom positions of the left and the right dots, $\pm a$. Compared with the case in which the impurity is located along the z direction, the considered case has a minimum around the point $x_1 \approx 2l_0$ (see Fig. 9) which is identical to the analytical minimum obtained using the Heitler–London approximation (see Appendix B). We note that such a minimum is obtained for an *attractive* impurity which has a positive charge $Z_1 < 0$ and $|Z_1| \ll 1$. Moving the impurity out of the dot system (blue dashed-dotted, red dashed, and cyan dash-dotted-dot curve in Fig. 9) will lead to a decrease in J. This situation can be considered as the coupled QDs interacting with charged impurities found close to the surface during the growth process. In particular, the case in which the impurity y coordinate is displaced to $0 < y_0/l_0 \ll 1$ has only a small difference in J from the case in which the impurity is positioned exactly along the x axis, $y_0 = 0$ (see the green short-dotted curves and solid black curves in Fig. 9).

2. *Impurity charge dependence*

The above critical point $x_1 \approx 2l_0$ at which the singlet-triplet splitting exhibits a maximum or minimum (see Fig. 9) depends on the effective impurity charge Z_1 and the well barrier height V_b. In this subsection, we examine the Z_1 dependence of the singlet-triplet spin splitting J.

Besides, we notice the physics sampled around the origin in Figs. 8(d) and 9(b), where the presence of a repulsive charged impurity significantly lowers the singlet-triplet spin splitting J. It is expected that, by further increasing the impurity charge Z_1, the system can be visited in the triplet state, i.e., $J < 0$.

Such triplet-singlet transition occurs as Z_1 is larger than $\approx$ 0.55. In both cases the impurity is located along the z axis and along the x axis as shown, respectively, in Figs. 10 and 11. Our calculations for the attractive coupling case $Z_1 < 0$ show that there is no triplet-singlet transition (see Figs. 10 and 11) due to the fact that a positively charged impurity attracts both electrons; therefore the favored spin state is always the singlet.

The triplet-singlet transition is further explored for different negative charges $Z_1 > 0$ as seen in both Figs. 10(a) and 11(a) for different impurity locations: at the center [black solid curve in Fig. 10(a) and full rectangles with black solid curve in 11(a)] and off-center – slightly away from the origin. We examine the triplet-singlet transition only for the systems with the e-I coupling smaller than or compatible with the e-e interaction. In fact, the limit of $Z_1 = \pm 1$ does not bear much physical meaning. However, we theoretically examine that limit to support a complete understanding of the effective e-I strength on the exchange electron qubits in the zero B field.

It is undoubted that when the impurity equally interacts with the two-QD electrons and the e-I interaction strength is considerable, the triplet ground state occurs at a smaller Z_1, compared with the unequal electron(s)-impurity interaction case. This argument is clarified in, e.g., Fig. 11(a), where the singlet state occurs by increasing Z_1 to $\approx$0.54 for $R_1 = 0$ and further up to 0.7 for $R_1 = a_m/4$ ($\approx 0.43l_0$). On the other hand, at a certain strong enough Z_1, the triplet state in the case when the impurity is located along the x axis remains longer than in the case when the impurity is located along the z axis. For example, for $Z_1 = 1$, we obtain that the triplet state stays up to $x_1 \approx 0.6l_0$ while it is found only up to $z_1 \approx 0.46l_0$. It is worth noting that, at a higher $V_b = 35$ meV, due to the influence of the impurity potential, the triplet state remains up to a larger

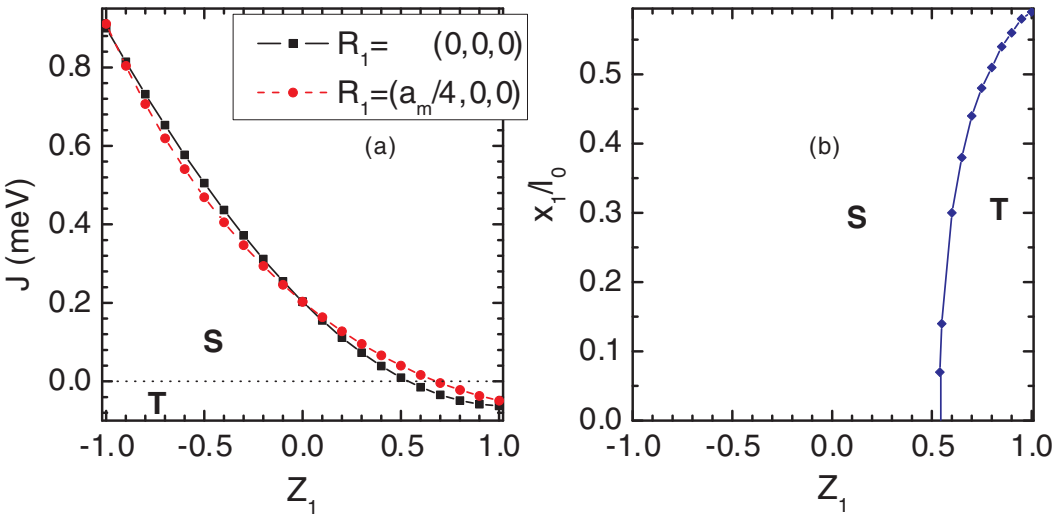

FIG. 11. (Color online) (a) Singlet-triplet spin splitting of a coupled two-dot system as a function of the effective charge Z_1 within the range $-1 < Z_1 < 1$ for $x_1 = 0$ (full squares with black solid curve) and $x_1 = a_m/4$ (full circles with red solid curve). (b) Singlet-triplet state diagram plotted in the impurity-position−effective-charge $R_1 - Z_1$ plane. V_b is taken to be 30 meV. Horizontal dotted line in (a) is used to clarify the triplet-singlet transition. In the region close to the center of the system, at $\approx 0.07 l_0$ (about $0.04 a_m$), a relatively large repulsive impurity potential, say $Z_1 = 0.54$, is enough to induce a triplet-singlet transition [see the state diagram (b)]. The stronger the effective charge, the broader the triplet region. Consequently, when moving the impurity close to the right bottom it requires a larger Z_1 to observe the triplet-singlet transition occur. S and T stand, respectively, for the singlet and triplet states.

x_1 in comparison with the 30-meV case. For example, such a triplet-singlet transition is obtained at $x_1 = 0.42 l_0$ and $0.72 l_0$ for $Z_1 = 0.6$ and 1, respectively.

When the impurity is located at the right well bottom for $Z_1 = \mp 1$, the ground state is always a singlet; however, the maximally entangled component ψ_1^S is replaced by one of the two double-occupied components $\{\psi_2^S, \psi_3^S\}$ as the major contribution to the total wave function.

We summarize in Figs. 10(b) and 11(b) the occurrence of the triplet or singlet as the ground state when changing the impurity position R_1 and its effective charge Z_1 for $V_b =$ 30 meV. The triplet state starts to occur when Z_1 is increased to ≈ 0.54 at $R_1 = 0$. The largest triplet region [$R_1 = (0, 0.38 l_0)$ in Fig. 10(b) and $(0, 0.6 l_0)$ in Fig. 11(b)] is, apparently, seen for the largest considered Z_1 (=1). In particular, close to the origin, the triplet region is rapidly shortened. For example, for $Z_1 = 0.6$ the triplet region is in $R_1 = (0, 0.3)$, while such a region squeezes to (0,0.07) as Z_1 decreases to 0.54. Note that we show the singlet-triplet state diagram on the right half of the x (z)axis. As the impurity is positioned along the other half of the x (z)axis, the state diagram is found similarly.

3. *Interdot separation dependence*

In this subsection, we study the interdot dependence of the singlet-triplet splitting J. First, we place the impurity at the center of the dot system, i.e., $\mathbf{R}_1 = (0,0,0)$, and tune the barrier height from $V_b = 35$ meV down to 13 meV. In the meantime, the interdot separation ($2a_m$) will decrease from $2a_m = 35$ nm ($\approx 3.5 l_0$) to 17 nm ($\approx 1.6 l_0$). It is worth noting that the case in which the impurity is placed exactly at either of the two well bottoms does not have any physical meaning in this case because the bottoms of the double well change concomitantly with V_b changing (see Fig. 1). In fact, the impurity position should be fixed; thus its position varies relatively only with respect to the double-well minima of different V_b systems. Consequently, different V_b two-dot systems exhibit various impurity effects on J. We obtain the interdot separation dependence of the singlet-triplet spin splitting J for $Z_1 = -0.1$ in Fig. 12 and $Z_1 = 0.1$ in Fig. 13.

For $Z_1 = -0.1$, the splitting energy J becomes smaller as the interdot separation increases (see Fig. 12). However, J is found larger than that of the case without charged impurity, as illustrated in, e.g., the full rectangles with the black solid line ($R_1 = 0$) and open rectangles with magenta short dashed line (no impurity) in Fig. 12. In this case, this means that the potential-well height is "weakened" by the attractive impurity which attracts the electrons toward and therefore supports the antiparallel spin interaction of the two electrons. Displacing the impurity away from the center of the double-dot system (full rectangles) along the x axis results in changes as seen in a series of J presented as full circles with a red solid curve (for $R_1 = 0.5 l_0$), full up-triangles with green dotted curve (for $R_1 = 0.7 l_0$), full down-triangles with blue solid curve (for $R_1 = l_0$), full rhombuses with dashed-dotted (for $R_1 = 1.5 l_0$), full right-triangles with yellow short-dotted curve (for $R_1 = 2 l_0$), full circles with dash-dotted-dotted curve (for $R_1 = 2.5 l_0$), and full stars with solid curve (for $R_1 = 3 l_0$). First, we analyze the data for the lowest case of $V_b = 13$ meV (corresponding to $2a_m \approx 1.65 l_0$). The minimum in J for this case is found at $x_1 \approx 1.3 l_0$[33] while the maximal value in J is always found at the origin $R_1 = 0$. Moreover, the system tends to covert to the nonimpurity situation when the charged impurity is engineered far enough from the center of the dot system. Therefore, from the $R = 0$ case to the $R = 0.7 l_0$ case we obtained such a decrease in J from ≈ 2.12 to 1.87 meV but for $R = l_0$ we obtained J almost identical to the J of a similar system but without impurity. Note that this impurity

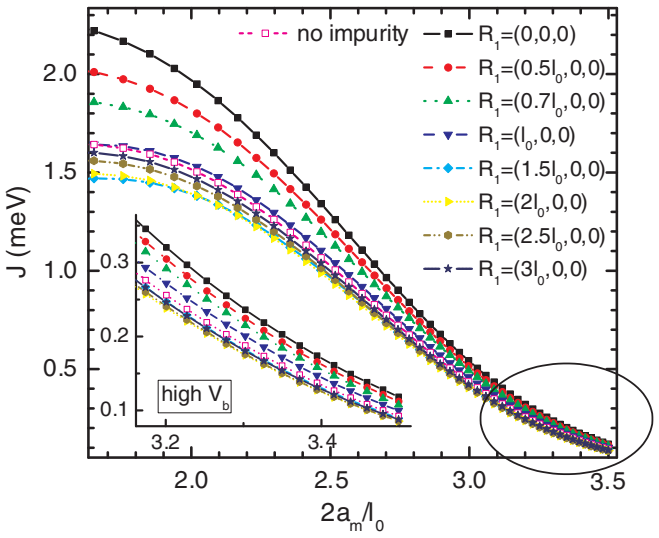

FIG. 12. (Color online) Singlet-triplet splitting energy J calculated as a function of the interdot separation $2a_m$ for different positions of the impurity when it is located along the x axis for $Z_1 = -0.1$, $Z_2 = 0$. We added data in case no impurity is present as the open squares with the magenta dashed line. Because V_b changes (from 35 down to 13 meV), effectively controlling the interdot separation, i.e., a_m, while the impurity position should be fixed during the V_b modification, we examine different locations of the impurity. Several examples of corresponding $(V_b, 2a_m)$ are (35 meV, $3.5l_0$), (30 meV, $3.3l_0$), and (25 meV, $2l_0$). Inset is the magnification of the region sampled by the big open circle for the high-V_b limit.

position l_0 is considered still close to the right bottom of the well barrier. This feature is similar to the physics around the impurity position $R \approx 1.2l_0$ for $V_b = 30$ meV as previously examined in full squares with the black solid curve in Fig. 9. Further increasing x_1 to $1.5l_0$ and $2l_0$ (as seen in the full rhombuses with cyan dashed-dotted and full right triangles with short-dotted cureves, respectively) we obtain the increase back in the latter case. This is found due to the fact that both $1.5l_0$ and $2l_0$ are located on the right-hand side of the minimal point in J. The latter case exhibits an increase because the system to this extent tends to convert to the nonimpurity case. In the furthermost case $R_1 = 3l_0$ (full stars with solid line), J is found closer to that of the nonimpurity case, which has higher energy than the cases $R_1 = 1.5l_0, 2l_0$, and $2.5l_0$.

Such a shift in the maximum of J by changing V_b can be seen in Fig. 12 and its inset for the high-V_b limit where the furthermost impurity positions $R_1 = 1.5l_0, 2l_0, 2.5l_0$, and $3l_0$ stay closer to the nonimpurity case in comparison with the small-V_b cases. This is related to the fact, which was mentioned above, that the relative distance of the impurity position to the minimal point of J varies where the impurity can be found either in the left- or the right-hand side of the minimal J as V_b changes. For $V_b = 30$ meV (corresponding to $2a_m \approx 3.3l_0$), from the center $R_1 = 0$ to the l_0 case the singlet-triplet spin splitting stays higher in energy while the others ($R_1 = 1.5l_0, 2l_0, 2.5l_0$, and $3l_0$) have lower J than the nonimpurity case. The minimal point for this system is $\approx 2l_0$. Therefore, the $R_1 = 1.5l_0$ case has a higher J than the $R = 2l_0$ case, which was opposite in the previous case, $V_b = 13$ meV. As a consequence, there appear crossings in J for different R_1. Obvious crossings are seen for the cases $R_1 = 1.5l_0, 2l_0, 2.5l_0$, and $3l_0$. For example, J for the $R_1 = 0.5l_0$ case (full rhombuses with cyan dashed-dotted curve) stays lower in energy; however, it changes as V_b varies and is found higher (or equal) in energy than the J in the others (see the inset as a magnification for the high-V_b limit).

Apparently, when placing the impurity close to the origin, we always obtain a larger singlet-triplet spin splitting compared with the nonimpurity case. The largest case has $\Delta J \approx 0.6$ meV for $R_1 = 0$ and $V_b = 13$ meV. It is worth noting that a larger V_b results in a smaller difference in J which can be understood as a lower "tunneling" rate of the two electrons in the two separate QDs. Quantitatively, such a decrease can be roughly estimated by Eq. (B1).

It was made clear in the presence of an attractive charged impurity the e-I coupling increases the tunneling rate between the two dots. Positioning the impurity at different locations inside the coupled two-dot system, in particular around the $(x_1 \approx 2l_0, 0)$ point, gives rise to different V_b-dependent singlet-triplet splitting which has crossings between different R_1 curves. As illustrated now in Fig. 13 for the $Z_1 = 0.1$ case, J in the $R_1 = 0$ case (full squares with black solid curve) stays lowest in energy and the J difference compared with the nonimpurity case is found largest. For example, $\Delta J \approx 5.5$ meV for $V_b = 13$ meV. J in the furthermost case, $R_1 = 3l_0$ (full stars with navy solid curve), stays slightly above the nonimpurity curve (open squares with magenta short-dotted curve). This implies that such an impurity position is on the right-hand side of the maximum point in J for all the considered V_b [$\in$(13, 35) meV] in Fig. 13. It is found opposite to the $Z_1 = -0.1$ case where the $R_1 = 3l_0$-J curve stays slightly lower than in the nonimpurity one. Crossings between different R_1-dependent J curves are still obtained in the current case $Z_1 = 0.1$, e.g., the one around $2a_m = 2.1l_0$ (corresponding to $V_b = 15.5$ meV) between the l_0 (full down-triangles with blue solid curve) and the $3l_0$-J curves, or the

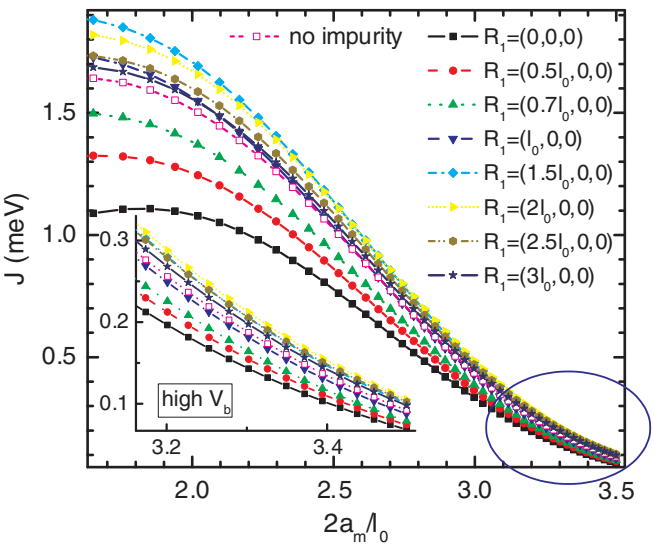

FIG. 13. (Color online) The same plot as Fig. 12 for $Z_1 = 0.1$. As the impurity position is engineered farther away from the origin, the double-dot system reveals crossings between different J for different R_1.

one at $2a_m \approx 2.61l_0$ ($V_b = 20$ meV) between the $1.5l_0$ (full rhombuses with cyan dashed-dotted curve) and the $2l_0$-J curve (see also the inset of Fig. 13), etc.

It is important to note that the $|Z_1| = 0.1$ case studied so far has not exhibited any crossing between the singlet and triplet states, i.e., the triplet state always stays higher in energy than the singlet state. The presence of an attractive impurity increases the singlet-triplet splitting as opposed to the effect seen for a repulsive impurity. The extreme behavior of J is obtained at either of the two minima of the potential well. An attractive impurity seems to increase the tunnel rate of the coupled-double-dot system.

B. Energy spectrum

In the single QDs, as discussed in Sec. III, the impurity effect on the energy spectrum of the system is substantial as e-I interaction is competitive with the e-e interaction. We obtained different crossings between low-lying excited states and anticrossings with varying energy gaps. If such a similar effect is found in the coupled-double-QD system, the question of "whether quantum operations in the coupled-dot system are affected" attracts our attention.

To examine the validity of using coupled dots containing charged impurities as the basis of quantum logic gates in quantum computation, we mainly look into the low-level energy spectrum.

The energy spectrum of double QDs containing a single impurity located at $\mathbf{R}_1 = (0,0,z_1)$ and $(0.5l_0,0,z_1)$, respectively, is shown as solid and dash-dotted curves in Fig. 14(a). The latter case (dash-dotted curve) has a larger impurity effect on the energy gap between the first two lowest levels and the two highest energy levels which can be understood from an earlier discussion. The energy levels bend down to the $z_1 = 0$ as its x coordinate $x_1 \neq 0$ as compared with the case $x_1 = 0$ because the impurity has a stronger interaction to the electrons when it is closer to the well bottoms.

The x_1 dependence of the energy spectrum is studied in Fig. 14(b) for two different $z_1 = 0$ and $z_1 = l_0/2$. The minimum, discussed earlier in Fig. 9, related to the physics of having an impurity around the well bottoms, is seen in the energy levels of Figs. 14(b) for $z_1 = 0$. The spin splitting between the two fully filled states is most affected also when the impurity is at the well minima. The probability of finding the two electrons in the right dot (containing the impurity) increases. The absolute value of the e-I coupling for the right (in the present case) doubly occupied state is maximal at $(a_m,0)$.

For $Z_1 = 0.1$ [see Fig. 15(b)], it is found opposite to the attractive $Z_1 = -0.1$ case. The impurity (in the right dot) now tends to repel both electrons which leads to a higher probability of finding the two electrons in the left dot. Consequently, the doubly occupied state of the right dot gains energy via the e-I interaction and stays higher in energy (blue dashed-dotted curve) than the singlet state (green dotted curve) of the left dot. Such a maximum around the bottom $(a_m,0)$ in the blue dashed-dotted curve in Fig. 15(b) has physics similar to that discussed earlier for $Z_1 = -0.1$. Remember that, in the attractive case, the singlet-triplet spin splitting has a minimum around $2l_0$ (see Fig. 9) which results due to i) the competition between the wave function overlap of the coupled two-dots and the impurity potential on the right-dot electron and ii) the doubly occupied states have a relatively small contribution to the total singlet state (the ground state). Now, the effective charge changes its sign (0.1) and we obtain a maximum [see the inset of Fig. 15(b)]. The other left-dot fully occupied state [green dotted curve in Fig. 15(b)] shows a decrease only in x_1.

Even though the presence of the impurity changes the singlet-triplet splitting, as discussed above, the energy gap $\Delta\epsilon$

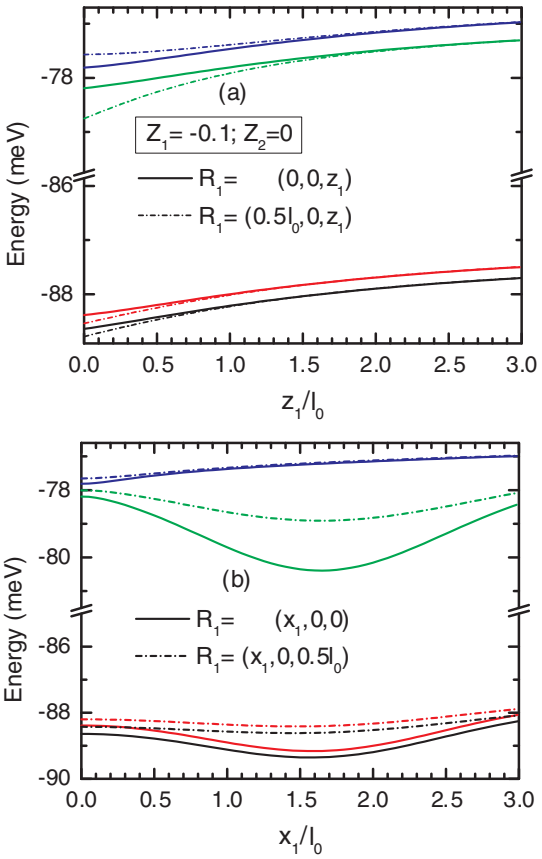

FIG. 14. (Color online) Energy spectrum of the QD system studied (a) in Fig. 8(a), and (b) in Fig. 9(a), respectively, as a function of the impurity position (along the z and the x axes) for $Z_1 = -0.1, Z_2 = 0$. $V_b = 30$ meV. Because there is no crossing or anticrossing in the energy spectrum, we use the same style of line for a certain R_1 dependence. In (a), solid curves depict the impurity-position dependence when the impurity is located along the z axis and, dash-dotted curves depict the situation when the impurity is outside the double-dot system [along the line $(y_1 = 0; x_1 = 0.5l_0)$]. In (b), solid curves depict the case R_1 when is changed along the x axis, and dash-dotted curves depict the situation where the impurity is outside the double-dot system but along the x direction. The latter case of (a) with $x_1 = 0.5l_0$ (dashed-dotted curves) reveals a stronger impurity effect on the coupled qubits in comparison with the case when the impurity is on the z axis [solid curves in (a)]. The $R_1 = (0,0,z_1)$ case induces equal exchange coupling to the two electrons mostly found on the individual dots. The latter case of (b), on the other hand has a much weakened impurity effect on the double-dot system in comparison with the case where the impurity is found on the line connecting the two confining potential minima.

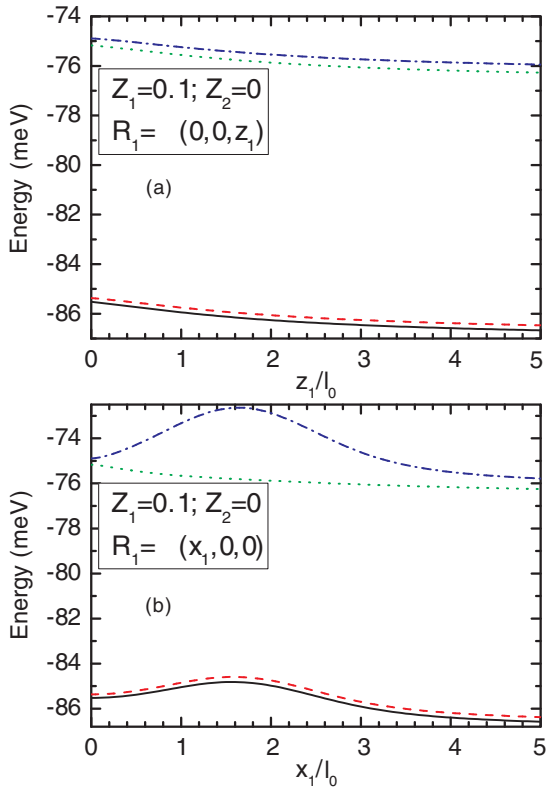

FIG. 15. (Color online) The same plot as shown in Fig. 14 for a repulsive impurity $Z_1 = 0.1$. There is a change in the relative order of the two excited states in (b) as compared to the above case $Z_1 = -0.1$ (see Fig. 14).

between the highest spin state that stores information and the lowest unwanted state, in this case the first- and the second-excited states, remains much larger than the singlet-triplet splitting energy J. In the case $V_b = 30$ meV, $J/\Delta\epsilon$ is typically $\leqslant 0.07$. This means that the adiabatic condition is satisfied so that higher excited states are not involved when the system is evolved to its desired state.

C. Strong electron-impurity coupling destroys coupled qubits

1. Strong perturbation

In the following, we discuss in detail the influence of a strongly perturbative impurity on the energy spectrum for $Z_1 = \mp 1$. Results for other intermediate Z_1 (e.g., ∓ 0.6, ∓ 0.8) are collected in Appendix C.

We plot in Fig. 16 the impurity-position dependence of the singlet-triplet spin splitting J when the impurity is located along the z axis for (a) $Z_1 = -1$ and (b) $Z_1 = 1$. The former case has a qualitative curve similar to the case $Z_1 = 0.1$ with a much larger exchange energy J. The latter case has a triplet-single transition which occurs at $z_1 = 0.38 l_0$ as obtained already in the singlet-triplet state diagram, Fig. 10(b). This property results from the strong e-I interaction as Z_1 is increased to 1.

For the case in which the impurity is located along the x axis and $Z_1 = 1$, we obtain in Fig. 17 and its inset the entire triplet state for the case in which the impurity is engineered at the origin or very close to the origin, say $R_1 < 0.6 l_0$ (see the inset). The $R_1 = 0$ case has the impurity that equally repels the two electrons in the two individual QDs and the impurity is kept distant from the two well minima. As a result, the favored state becomes the triplet with two electron spins aligned parallel to each other. Moving the impurity off-center means that there appears a bias in the impurity-electron coupling with the two electrons. Such a triplet state becomes weakened and disappears when the bias increases to its maximum for the case when the impurity is found around the bottoms of the confining potential.

2. Destroy of coupled qubits

The impurity effect of small effective charges shown in Figs. 9 and 15 as discussed above for $Z_1 = \mp 0.1$ results in a relatively small coupling between the three Hund–Mulliken singlets in the ground-state singlet. Quantitatively, the major ($\approx 98\%$) component is the ψ_1^S; therefore the mixing of ψ_1^S with the other two singlets $\psi_{2,3}^S$, with the probability of about 1% each, can be neglected. The considerable impurity effect

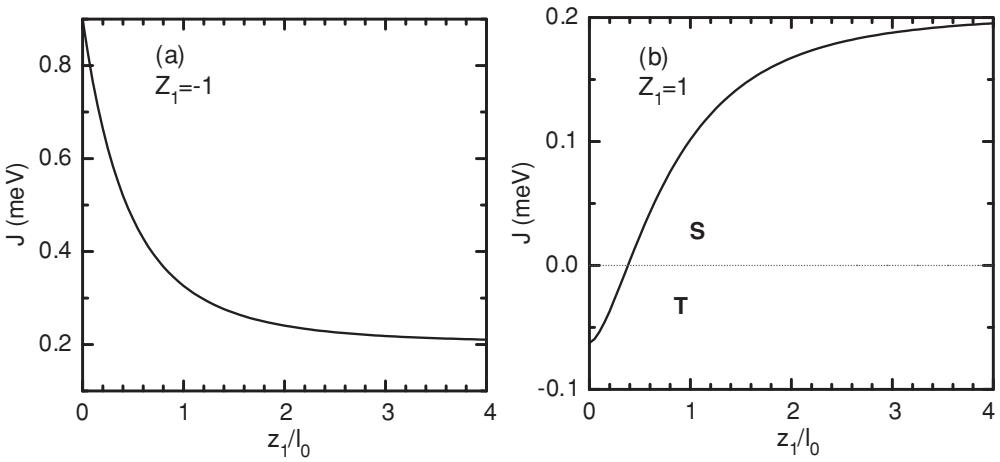

FIG. 16. Singlet-triplet spin splitting J calculated as a function of the impurity position along the z axis for (a) $Z_1 = -1$ and (b) 1. $V_b = 30$ meV. S and T stand for, respectively, singlet and triplet. The horizontal dotted line in (b) is used to clarify the triplet and singlet states. Such a triplet-singlet transition is obtained at $z_1 = 0.3 l_0$ for Z_1=1.

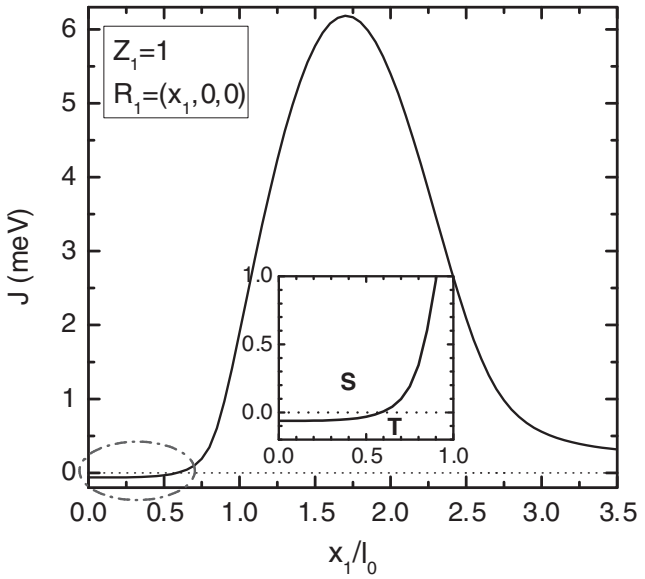

FIG. 17. Singlet-triplet spin splitting J of a singly doped charged impurity coupled-double-dot system as a function of the impurity position when it is located along the x axis for $Z_1 = 1$. $V_b = 30$ meV. The inset is the magnification of the circled region in the main plot which highlights the triplet-singlet transition in the small-x_1 region.

is observed in the excited singlets where such full bonding and antibonding states are no longer found at $B = 0$ when the impurity is found in either of the two individual QDs. Plus, the probability of finding the electrons in a fully occupied state is increased.

In the next examination, we study the case when the coupling between the electron and the impurity is compatible with the electron-pair Coulomb interaction by increasing the absolute effective impurity charge Z_1 to ± 1. The energy spectra are now shown in Figs. 18(a) and 18(b). For the attractive impurity case [see Fig. 18(a)], the triplet remains as the first-excited state while the ground state now mixes three singlets, with the leading term varying either the spin exchange singlet, Ψ_1^S, or the right-dot doubly occupied state ψ_3^S. The other singlet ψ_2^S (left dot) has a slightly larger than zero contribution.

Particularly, the singlet-triplet splitting in the case $Z_1 = -1$ changes mostly differently in comparison with the weak-impurity-potential case $Z_1 = -0.1$. J now has somewhat similar physics to the case $Z = 1$ around the right bottom of the potential well. A maximum in J ($\approx$6 meV) was seen in both cases, as shown in the insets of Figs. 18(a) and 18(b).

Now, the strong e-I interaction leads to the triplet-singlet transition at $R_1 \approx 0.6 l_0$ (as discussed already) for $Z_1 = 1$ and "virtual" coupling between the three states ψ^T, ψ_1^S, and ψ_2^S with each other.

As compared with the weak-perturbative case, where the minor contributions of the $\psi_{2,3}^S$ states, up to 1% each, are negligible, such contributions now start increasing and can exceed 50% and even larger for the doubly occupied singlet of the dot containing the attractive impurity (the right dot, i.e., the ψ_3^S) and of the dot without impurity (the left dot, i.e., the ψ_2^S) for the repulsive case. Consequently, the doubly occupied state can become the ground state and the exchange spin singlet becomes the first excited singlet. From Fig. 18(a), the green short dotted curve corresponds to the ψ_3^S (major) and the blue dashed-dotted curve corresponds to the ψ_2^S (major)

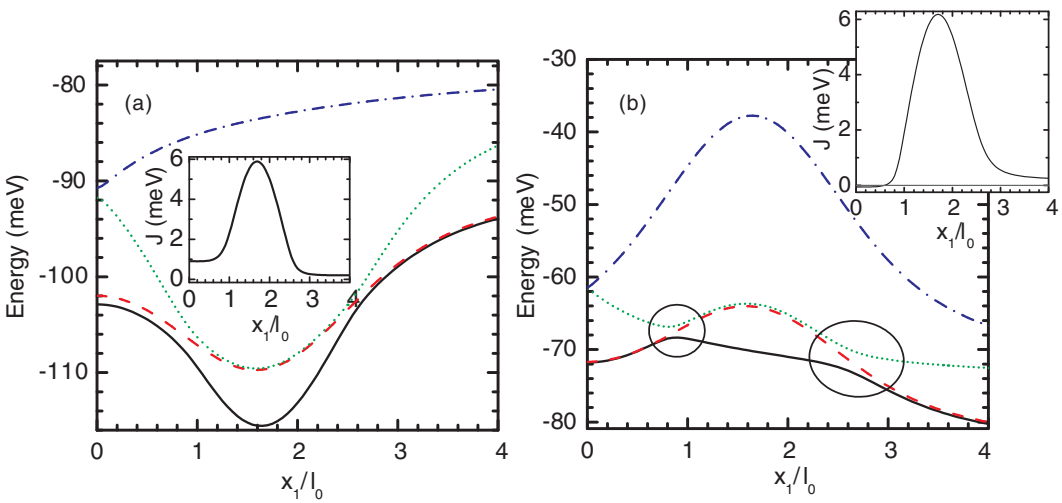

FIG. 18. (Color online) Energy spectrum of a coupled-QD system exhibits a strong impurity effect examined as a function of the (single) impurity position located along the x axis for a (a) positively ($Z_1 = -1$) and (b) negatively ($Z_1 = 1$) charged impurity. The inset in each layer is the corresponding singlet-triplet spin splitting J where both exhibit a maximum around the right bottom of the well. Different from the attractive case $Z_1 = -1$ in (a), the repulsive case $Z_1 = 1$ in (b) overcomes a triplet-singlet transition at $\approx 0.6 l_0$ [see the inset of (b)]. The green dotted curve in (a) represents either the ψ_3^S singlet or the ψ_1^S singlet (see discussion in text) while the green dotted curve in (b) represents either the ψ_2^S singlet or the ψ_1^S singlet. The red dashed curves in both (a) and (b) are the triplet states. Circles that sample the anticrossings indicate the transition of ψ_1^S as the ground state to the first excited state and the transition back to the ground state as x_1 increases. Anticrossings and an almost zero-energy gap between the first and second excited states in both (a) and (b) are the evidence to claim that the coupled qubits are "destroyed" and the adiabatical condition is violated.

state in the region $R_1 < 0.8l_0$ and $R_1 > 2.7l_0$. The region in between $0.8l_0 < R_1 < 2.7l_0$ has the ground state as the doubly occupied singlet ψ_3^S in Fig. 18(a) and ψ_2^S in Fig. 18(b). The minor components in the first-excited state in both cases, respectively, ψ_1^S plus ψ_3^S and ψ_1^S plus ψ_2^S, fluctuates around 7% and 3% as the impurity is located close to the center of the system. In Fig. 18(b) we see a switch between the left and right doubly occupied singlets where the singlet of the right dot (with impurity, blue dashed-dotted curve) stays higher in energy than the one of the left dotted curve (green dotted curve).

The "virtual" coupling between the three singlets and the triplet addressed above is now examined in both cases $Z_1 = \mp 1$. At the well right bottom $R_1 = (a_m,0)$, the triplet (red dashed curve) "couples" with the first excited singlet as the green dotted curve [ψ_3^S in Fig. 18(a)] and [ψ_2^S in Fig. 18(b)]. The energy gap between the triplet and the first-excited state is found close to zero. This virtual coupling can be understood by the two anticrossings between ψ_1^S and ψ_3^S in Fig. 18(a) and between ψ_1^S and ψ_2^S in Fig. 18(b).

To better understand the physics manifested in the mixing of different singlet states as well as the "coupling" between the triplet and the first-excited singlet as shown in Figs. 18(a) and 18(b) and the triplet-singlet transition in case $Z_1 = 1$, we calculate the probability of finding the three singlet states as functions of the impurity position inside the double-dot system for weak and strong e-I coupling, respectively, in Figs. 19(a) and 19(b) and Figs. 19(c) and 19(d) for the ground state. We first explain for the triplet-singlet transition in the case $Z_1 = 1$ [see Fig. 17(a)] and the "coupling" of the first excited singlet and the triplet in case $Z_1 = \mp 1$ [see Figs. 18(a) and 18(b)]. The triplet-singlet transition can be understood from Fig. 19(d), where the region $x_1/l_0 \leqslant 0.6$ has zero probability of finding the ψ_1^S state in the ground state. It is because the triplet state becomes the ground state and the singlet ψ_1^S is the major component of the first-excited-state wave function in this considered region. The dominant of the doubly occupied singlet ψ_3^S in the ground state for $Z_1 = -1$ and of the ψ_2^S for $Z_1 = 1$ is now specified as the region $0.8l_0 < x_1 < 2.7l_0$ in Figs. 19(c) and 19(d). This region is identical to the maximal behavior of J as seen in Figs. 18(a) and 18(b) and their two insets. For the weak-impurity-potential cases $Z_1 = \mp 0.1$, there are no anticrossings in the energy spectrum and the doubly occupied singlets remain always as the excited singlets with small probability [see Figs. 19(a) and 19(b)].

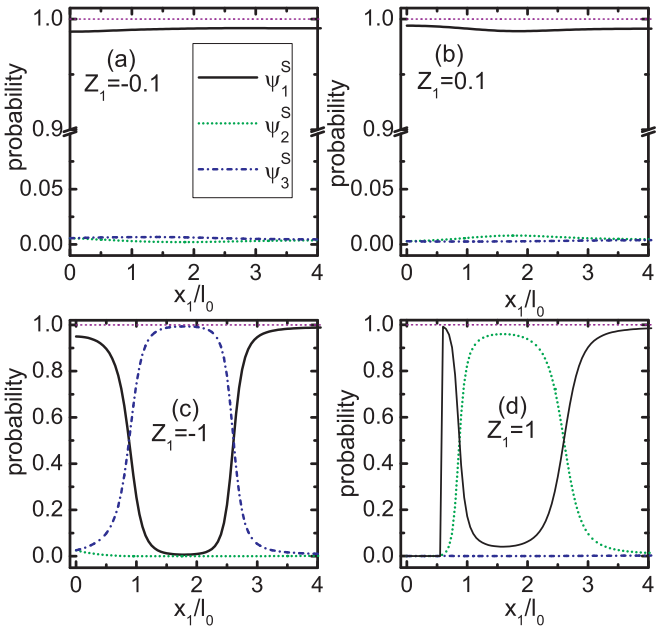

FIG. 19. (Color online) Probability of finding the three singlet states as defined in Eq. (17) in the ground state as a function of the impurity position for different Z_1 for weak (a) [$Z_1 = -0.1$ and (b) 0.1] and strong (c)[$Z_1 = -1$ and (d)1] impurity potentials. The triplet state can be the ground state and only "couples" (e.g., via an anticrossing, as discussed earlier in Fig. 18) but does not mix with the singlet; states therefore the probability of finding such a state is always 1. The impurity position is $\mathbf{R}_1=(x_1,0,0)$. The top dash-dotted horizontal line corresponds to the probability of finding the Ψ_1^S state in the case without impurity for $B = 0$.

D. Coupled qubits perturbated by two impurities

For simplicity, we first assume that two impurities have identical charges $Z_1 = Z_2$ and one impurity is kept at one of the two minima $\mathbf{R}_2 = (-a_m,0,0)$. The other impurity can be arbitrarily located along the other side of the x axis, $\mathbf{R}_1 = (x_1 > 0,0,0)$. Under these circumstances, the two impurities generally induce different e-I couplings and hence affect the qubits asymmetrically except when $x_1 = -x_2 = a_m$(See Fig. 20). In this case, both doubly occupied singlets are found compatible which have similar contribution to the two excited singlet states. Therefore we no longer see a minimum or maximum, depending on the sign of Z_1, in the second- or third-excited state as obtained in the case $Z_2 = 0$. Such a pronounced minimum is now "eliminated" due to the presence of the second impurity, located at the other bottom (left) of the two-dot system, which induces a competing e-I coupling. The singlet-triplet spin splitting J has maximal behavior when the impurity is found close and at the bottom of the right dot.

Another way to study the asymmetric impurity effect in the considered double-dot system with two impurities is to adjust the effective impurity charges with respect to each other while their positions are kept symmetrical to the origin, i.e., $Z_1/Z_2 \neq 1$ while $\mathbf{R}_1 = -\mathbf{R}_2$. We compute the singlet-triplet spin splitting for three different values of $Z_2/Z_1 = 1, 1.1$, and 1.2, while $R_{1,2}$, changes for both the positively and negatively charged cases in Figs. 21(a) and 21(b), respectively. The results shown in Fig. 21 are obtained for Z_2/Z_1 slightly different in units to examine the asymmetry that arises due to the dissimilarity in impurity charges compared with the asymmetry due to the impurity positions discussed earlier in Fig. 20 for $Z_1 = Z_2$.

Apparently, if one replaces one of the two identical impurities by an charge opposite to the other, one can revisit the "asymmetric" phenomenon between the two doubly occupied singlets in the two dots which now can be enhanced as a double. Our further calculations show that if $Z_1 = -Z_2 = -0.1$ and $\mathbf{R}_1 = -\mathbf{R}_2 = (-a_m,0,0)$, for $V_b = 30$ meV the two doubly occupied states have a significantly large energy gap and the higher level, which is the right-occupied state in this case, exhibits a maximum around $(a_m,0)$, one of the two potential-well minima. Generally, this considered situation

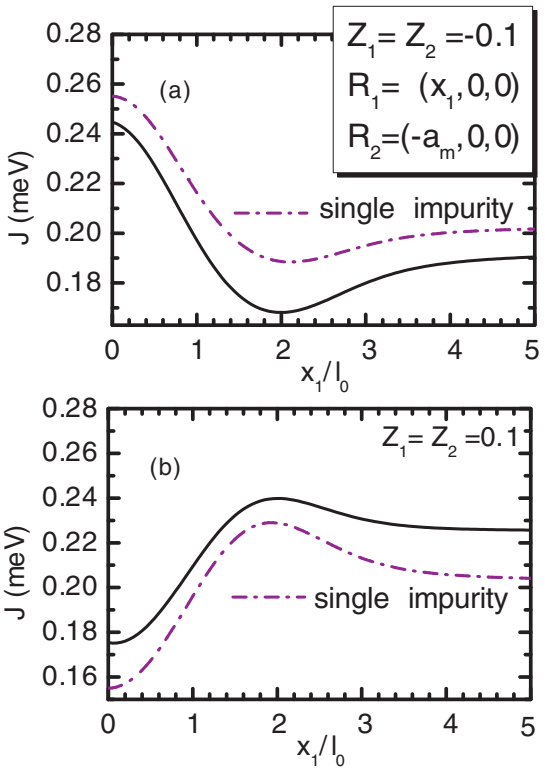

FIG. 20. (Color online) Singlet-triplet splitting (black solid curve) of a coupled-two-dot system with the presence of two identical charged impurities but located asymmetrically along the x axis: one is fixed at the left bottom and the other is located along the $x > 0$ axis for weak e-I coupling: (a) $Z_1 = Z_2 = -0.1$ and (b) $Z_1 = Z_2 = 0.1$. V_b is taken to be 30 meV. Violet dashed-dotted curves are the J for the single-impurity system extracted from Fig. 9.

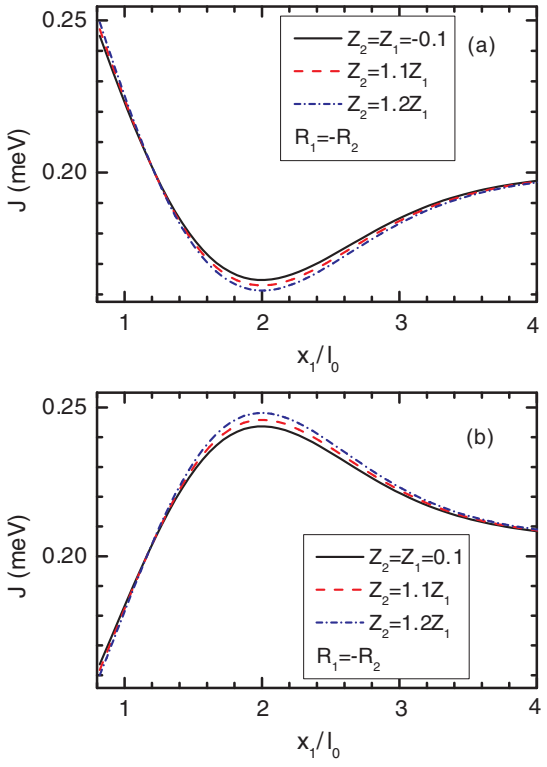

FIG. 21. (Color online) Singlet-triplet spin splitting J as a function of the impurity position in the case when the two impurities are symmetrically located, $\mathbf{R}_1 = -\mathbf{R}_2$, but they are charged slightly differently: (a) both impurities are positively charged and (b) both impurities are negatively charged with $Z_1 = \pm 0.1$ and $Z_2 = Z_1$ (black solid curve), $1.1Z_1$ (red dashed curve), and $1.2Z_1$ (blue dashed-dotted curve). V_b is taken to be 30 meV. V_b is fixed at 30 meV, which corresponds to $a_m \approx 1.64 l_0$. Note that the system converts to the situation without impurity at a much larger x_1 than the singly doped impurity case (previously seen around $3.5 l_0$). In this plot, at $x_1 = 4 l_0$ the system does not convert to the case without impurity (e.g., $\Delta J \approx 0.01$ meV) and the total binding energy $\Delta E \approx .8$ meV for $Z_1 = -0.1$ [black solid curve in (a)].

can be extended to the case in which the charged impurities are different types and obey a specified charge distribution. By examining the energy spectrum of the coupled dot, as illustrated in the above discussion, one can detect the impurity effect on the singlets of the double-dot system. This can be made possible due to the distinguishability between the total positively and the total negatively charged cases. It is also possible that both impurities are found either in the left or right dot; however, not much different physics from the case with only a single impurity will be added.

The last part of this section is reserved to examine one special case described in what follows. The coupled two-dot system interacts with two negatively charged impurities $Z_1 = Z_2 = 1$, equal to the electron charge. Now, the two impurities are engineered such that they are far enough from the target (A) coupled two-dot sample and induce an electrostatic interaction only to the two electrons of the target system. We examine the case in which the two impurities have varied positions but their center-of-mass coordinates are kept unchanged, in this case $\mathbf{R}_{12}^c = (\mathbf{R}_1 + \mathbf{R}_2)/2 = (5a_m, 0, 0)$. This center-of-mass location can be imagined as another "center" of another coupled two-dot system (B) where the two impurities are mostly found at the well bottoms of system B. That the relative positions of individual impurities vary with respect to their center-of-mass position can be imagined as the well barrier height is tuned, resulting in varying interdot separation in system B. A and B interact only via the e-I Coulomb interaction. Now, we study the influence of the presence of system B on the qubits of system A. We plot in Fig. 22 the singlet-triplet spin splitting as a function of one impurity position for system A. We find that J decreases as the impurity which stays closer to the system A is positioned further from the system A. This effect is expected to be significantly enhanced if one applies an external field to engineer the impurities in and out the active region of target system A. As a result, one can see such anticrossings as seen earlier for $Z = \mp 1$, where the triplet state stays in-between the two lowest singlets.

V. DISCUSSION AND CONCLUSION

The coupling of two qubits is sensitively affected by the presence of a charged impurity. A charged impurity which is found inside the right or the left dot "breaks down" the equality between the right and the left doubly occupied singlet states. In the case when the impurity weakly couples with the electrons, the maximally doubly occupied singlet of the dot

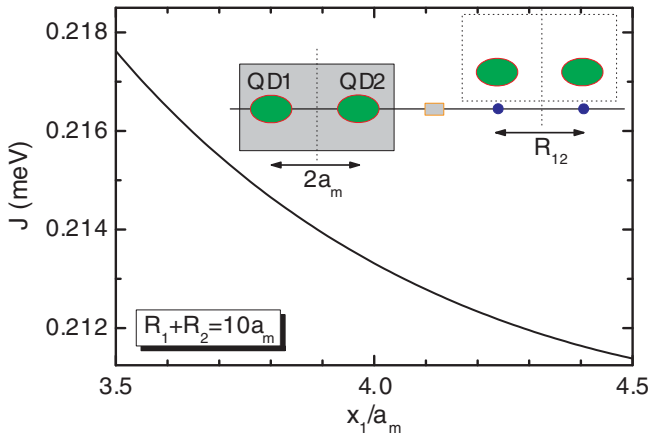

FIG. 22. (Color online) Singlet-triplet spin splitting J as a function of the impurity position in case the two impurities (blue circles) are located relatively far from the two potential minima, $\mathbf{R}_1 + \mathbf{R}_2/2 = 5a_m$ and the closest impurity to the active coupled two-dot system (the gray box) starts at $R_1 = 3.5a_m$. By fixing the center-of-mass coordinate of the two impurities at $R_c = 5a_m$, we imply such two impurities can be considered as another coupled two-dot system which has no tunneling coupling with the considered two-dot system in the gray box. That the relative positions of each impurity $\mathbf{R}_{1,2}$ vary with respect to the origin (0,0) of the active system can be mapped to the problem of other two-dot system (in open dotted box) with varying potential barrier heights. V_b of the active system is taken to be 30 meV. J is slightly different from that of the system without impurity.

containing the impurity has a smaller energy due to the e-I coupling. This can be considered as a tool to distinguish the doped and undoped QD components in the coupled-QD system.

A relatively strongly repulsive impurity which almost equally couples to the two individual QD electrons will result in an entire triplet state at B = 0 due to the small competition between the two e-I couplings. This can be observed by positioning the impurity around the origin of the double-dot system. When the impurity is found close to the bottoms of the confining potential well the system will stay in the singlet state where the two electrons perform the favored singlet state with spins anti-parallel to each other. Due to this fact, the influence of the interdot separation in the presence of impurity can be examined by modulating the well barrier V_b without changing the single-particle properties in individual QDs. The reason is that the relative position of the impurity with respect to the minima of the two-dot system is effectively controlled by changing V_b. We found that an attractive impurity serves to increase the "tunnel" rate between the two coupled dots.

In general, charged impurities "destroy" the maximally entangled singlet state by mixing the different singlets having varying contributions to the total wave function. A strongly perturbative impurity really "messes up" the quantum information obtained from this coupled QDs because the triplet state couples to the second-excited state by the presence of anticrossings with a slightly larger than zero-energy gap. The ground state now can favor a doubly occupied state. Because the triplet is always obtained with probability 1, it occurs in between the two lowest singlets: the exchange singlet ψ_1^S and the doubly occupied ψ_2^S or ψ_3^S depending on the sign of the effective charge Z_1. The energy spectrum appears with anti-crossings, as seen in our results.

In the presence of two identical charged impurities, the breakdown between the two doubly occupied singlets of the left and the right dots is "mended" if the impurities are located exactly symmetrically along the line connecting the two confining potential minima, i.e., the x axis. As a result, one no longer obtains such a bias between the two doubly occupied singlets in the left or the right dot, as seen in the energy spectrum.

The mixing of different singlet states and anticrossing coupling of the singlet and triplet states due to the impurity presence results in a significant effect on the qubit operations, e.g., exchange and C-NOT, in the considered coupled two-QD system.

Finally, we discuss the implications of our results for the operation of semiconductor spin qubits. Obviously, without some quantitative knowledge of impurity locations near the qubits, no real comparison between our results and experiments would be possible. But we can make some general remarks based on statistical considerations.

First, semiconductor qubits are typically fabricated by lithographic techniques, creating QDs from parent 2DEG systems. The low-temperature mobility of the 2DEG is controlled entirely by the background charged impurity density both in Si[34] and in GaAs[35] systems. Theoretical calculations[34,35] can provide quantitatively accurate information about the ensemble-averaged impurity density in the 2DEG from the mobility measurements. This information about the background impurity density can be converted to a statistical probability of finding impurities located in specific QD structures since the effective active areas of the dots would be known from the lithographic structures. For example, a typical GaAs 2DEG would have 10^{10} to 10^{11} charged impurities per square centimeter. whereas Si systems are typically dirtier with 10^{11} to 10^{12} charged impurities per square centimeter. This crudely translates to one charged impurity every 10 to 100-nm in linear distance statistically. Typical lithographic qubits are 20–100 nm squares, indicating the presence of 1-5 charged impurities per qubit statistically with GaAs (Si) being near the lower (higher) number. Of course, the details of impurity locations matter very much, and the statistical considerations could be improved and combined with our exchange splitting calculations to obtain the effective sample "yield" for a given 2DEG mobility, i.e., estimate the fraction of samples that would statistically have the impurities far enough for spin-qubit operations to work. But even these elementary considerations show that the effective yield is likely to be very low, with probably only about 1–5% of QD systems being "lucky enough" to have the impurities located far enough from the dots for them to work as spin qubits. The rest, even before taking into account extraneous experimental factors (e.g., leakage, noise), simply would not work because there is no effective singlet-triplet coupling providing the necessary entanglement in the system. A possible way of circumventing this problem may perhaps be having several electrons per dot so that the external charged impurity potential is effectively screened by the QD electrons, but this raises the problem of having rather weak exchange coupling in multielectron dots.[22]

The complex interplay of multielectron dots in the presence of random-charged impurities in the background is left as an important future open problem in this subject, which may very well be the next important step in this direction.

Second, an important effect of background charged impurities is their fluctuations which produce various charge-noise signals in semiconductor devices. This charge noise may very well be the limiting decoherence mechanism in currently existing semiconductor QD spin qubits.[36] Normally, of course, charge noise would not adversely affect spin configurations, but semiconductor spin qubits depend on the electrostatic exchange coupling which is affected by external charged impurities, as discussed extensively in this paper. Therefore, any impurity fluctuations would lead to spin-qubit decoherence through the charge-noise mechanism.[37,38] Our current work provides a quantitative estimate of the strength of such charge noise if the fluctuation spectrum (or the fluctuation time scale) is known. Deriving microscopic information about charge noise from our results could be another future interesting direction of research.

Third, the inevitable presence of static charged impurities in the background makes every semiconductor dot spin qubit, whether in GaAs or in Si (or some other material), unique since the microscopic electrostatic potential environment for each qubit will necessarily differ in a random manner from qubit to qubit due to background impurities, as shown in this paper. In particular, the singlet-triplet energy separation and the consequent exchange coupling will thus be somewhat random in a collection of many qubits. This would in turn necessitate characterization of each qubit in the eventual quantum computer rather precisely since the gate operations depend very strongly on the knowledge of the exchange coupling between the dots. Such a characterization will adversely affect the scalability of semiconductor spin quantum computer architectures. Our work shows the importance of having an ultraclean impurity-free environment even for solid-state quantum computation, similar to the requirements for topological quantum computation using non-Abelian fractional quantum Hall states,[39] not because spin quantum computation needs ultra high mobilities,[34] but because it requires stable values of exchange coupling without large qubit-to-qubit variations. Our current work indicates that an order-of-magnitude reduction in the background impurity concentration in GaAs, bringing it down to around $10^{13}/\mathrm{cm}^2$, which is also the goal for topological quantum computation,[39] should lead to the production of 100–1000 spin qubits with an impurity-free environment rather easily. Unfortunately, for Si-SiO_2 systems this is a very stringent condition because of the invariable presence of large oxide charges near the interface,[35] but for GaAs[34,36] and Si-Ge-based QD systems,[32,38,40] low-impurity materials may become available for quantum computer architectures in the near future.

Fourth, most of the spin-qubit manipulation experiments in semiconductor QDs are carried out under transport situations using an external dc voltage bias. Such external voltage affects the two dots differentially, somewhat similar to the impurity effects discussed in the current paper since the confinement potentials for the two dots are affected differently by the external voltage. Our technique can be used to study this effect. Another possible future direction of study could be impurity effects on the fully coupled-QD energy spectra (i.e., in addition to just the double-dot exchange energy mainly considered in the current paper) since in some experiments[41] higher energy levels come into play. It will, in fact, be interesting also in this context to consider multielectron QD systems with more than one electron per dot and ask how impurity disorder affects the energy spectra. This would necessitate a calculation of the QD electronic structure using many orbitals per dot (e.g., $s,p,d,f,...$), which is beyond the scope of the current work.

ACKNOWLEDGMENTS

This work is supported by LPS-NSA and IARPA.

APPENDIX A: COULOMB MATRIX ELEMENTS

1. Single QDs

To evaluate the e-I Coulomb matrix element, we calculate the integral:

$$V_{n_1 l_1}^{n_2 l_2}(\widetilde{R}) = \int \varphi_{n_1 l_1}^{*}(\widetilde{\mathbf{r}}) \frac{1}{|\widetilde{\mathbf{r}} - \widetilde{\mathbf{R}}|} \varphi_{n_2 l_2}(\widetilde{\mathbf{r}})\, d\widetilde{\mathbf{r}}, \tag{A1}$$

where $\varphi_{n,l}(\widetilde{\mathbf{r}})$ is defined in Eq. (7). The denominator on the right-hand side of Eq. (A1) is eliminated using the Gaussian identity:

$$\frac{1}{r} = \frac{2}{\pi} \int_0^\infty e^{-u^2 r^2} du. \tag{A2}$$

Integrating integral (A1) over θ and setting $\widetilde{r}^2 = t$, we arrive at

$$V_{n_1 l_1}^{n_2 l_2}(\widetilde{R}) = \delta_{l_1,l_2} \sqrt{\frac{n_1! n_2!}{(n_1 + l^+)!(n_2 + l^+)!}} \times \int_0^\infty t^{l^+} e^{-(1+u^2)t} L_{n_1}^{l^+}(t)\, L_{n_2}^{l^+}(t)\, e^{-u^2 \widetilde{R}^2} dt du. \tag{A3}$$

Next, we use one of the properties of the Laguerre polynomials[42]:

$$\int_0^\infty t^{\alpha-1} e^{-pt} L_m^\lambda(at)\, L_n^\beta(bt)\, dt = \frac{\Gamma(\alpha)(\lambda+1)_m(\beta+1)_n p^{-\alpha}}{m!n!} \sum_{j=0}^{m} \frac{(-m)_j(\alpha)_j}{(\lambda+1)_j j!} \left(\frac{a}{p}\right)^j \times \sum_{k=0}^{n} \frac{(-n)_k(j+\alpha)_k}{(\beta+1)_k k!} \left(\frac{b}{p}\right)^k$$

and the gamma functions for integers to calculate the integral on the right-hand side of (A3). Finally, we arrive at the formula presented in Eq. (18).

2. Coupled QDs

In general, the Coulomb matrix elements between the electrons and impurity are obtained numerically. Except for a few cases with applied constraint conditions to the impurity position, it is impossible to obtain a closed algebraic form for this type of Coulomb interaction. Using a similar method as

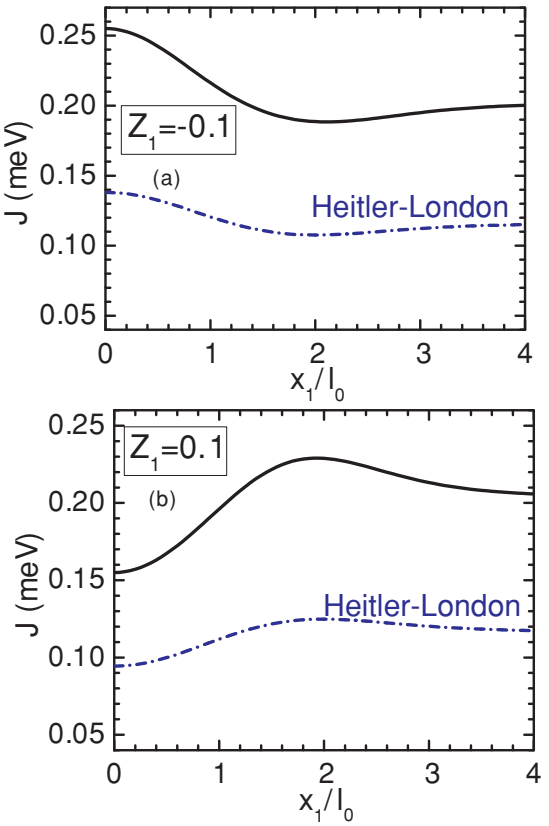

FIG. 23. (Color online) Singlet-triplet spin splitting J as a function of the impurity position along the x axis for (a) $Z_1 = -0.1$ and (b) 0.1. Black solid curves are extracted from Fig. 9 and blue dashed curves are obtained from Eq. (B1). We receive qualitative agreement between our numerical calculations and analytical results where the singlet-triplet splitting energy calculated using these two methods exhibits (a) a minimum a for $Z_1 = -0.1$ and (b) a maximum for $Z_1 = 0.1$ around $x_1 \approx 2l_0$.

before to calculate the e-I coupling elements, i.e., $\langle \Psi | \widehat{V}_{e-I} | \Psi \rangle$, we obtain

$$\begin{aligned} \langle \varphi_{L(R)} | V_{e\text{-}I} | \varphi_{L(R)} \rangle &= \frac{Z V_0^C}{\sqrt{\pi}} \int_0^\infty \frac{e^{-v z_0^2 - \frac{v}{v+1}}}{\sqrt{v}(v+1)} dv, \\ \langle \varphi_{L(R)} | V_{e\text{-}I} | \varphi_{R(L)} \rangle &= Z V_0^C \sqrt{\pi} e^{z_0^2 - a_0^2} \mathrm{erfc}(z_0), \end{aligned} \tag{A4}$$

for $\mathbf{R} = (0,0,z)$ and

$$\begin{aligned} \langle \varphi_{L(R)} | V_{e\text{-}I} | \varphi_{L(R)} \rangle &= Z V_0^C \sqrt{\pi} e^{-\frac{[(x_0 \pm a_0)^2 + y_0^2]}{2}} \\ &\quad \times I_0 \left[\frac{(x_0 \pm a_0)^2 + y_0^2}{2} \right], \\ \langle \varphi_{L(R)} | V_{e\text{-}I} | \varphi_{R(L)} \rangle &= Z V_0^C \sqrt{\pi} e^{-[a_0^2 - \frac{(x_0^2 + y_0^2)}{2}]} I_0 \left[\frac{(x_0^2 + y_0^2)}{2} \right], \end{aligned} \tag{A5}$$

for $\mathbf{R} = (x_0, y_0, 0)$, where $a_0 = a_m / l_0$, $x_0 = x/l_0, y_0 = y/l_0$, and $z_0 = z/l_0$.

It is of interest to consider the special situation when the impurity is located along the line connecting the two potential-well minima, i.e., along the x axis in this case. In the above sections, we discussed this case in depth. The Coulomb matrix elements for the left and the right QD electrons are as follows:

$$\begin{aligned} \langle \varphi_{L(R)} | V_{e\text{-}I} | \varphi_{L(R)} \rangle &= Z V_0^C \sqrt{\pi} e^{-\frac{(x_0 \pm a_0)^2}{2}} I_0 \left[\frac{(x_0 \pm a_0)^2}{2} \right], \\ \langle \varphi_{L(R)} | V_{e\text{-}I} | \varphi_{R(L)} \rangle &= Z V_0^C \sqrt{\pi} e^{-(a_0^2 + \frac{x_0^2}{2})} I_0 \left[\frac{x_0^2}{2} \right]. \end{aligned} \tag{A6}$$

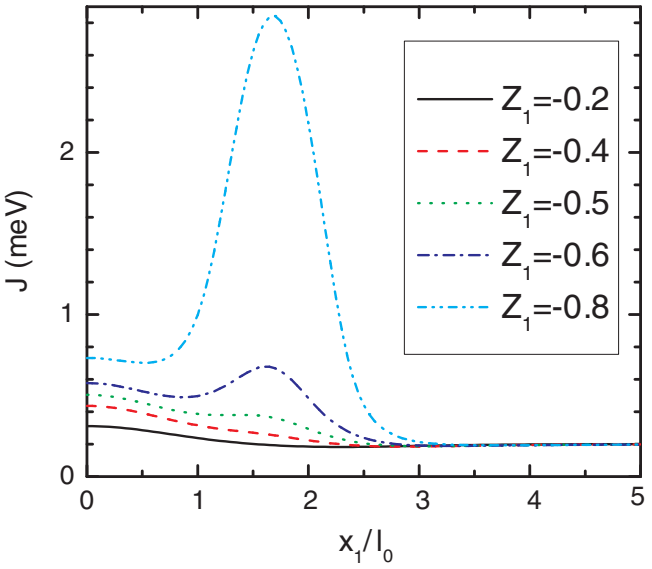

FIG. 24. (Color online) Singlet-triplet spin splitting J as a function of the impurity position along the x axis for different $Z_1 < 0$. In this plot one can see the gradual change in J from having a minimum around $x_1 \approx 2l_0$ to having a maximum at different x_1 depending on Z_1 as Z_1 is increased from -0.1 (black solid curve) to -0.8 (cyan dash-dotted-dotted curve).

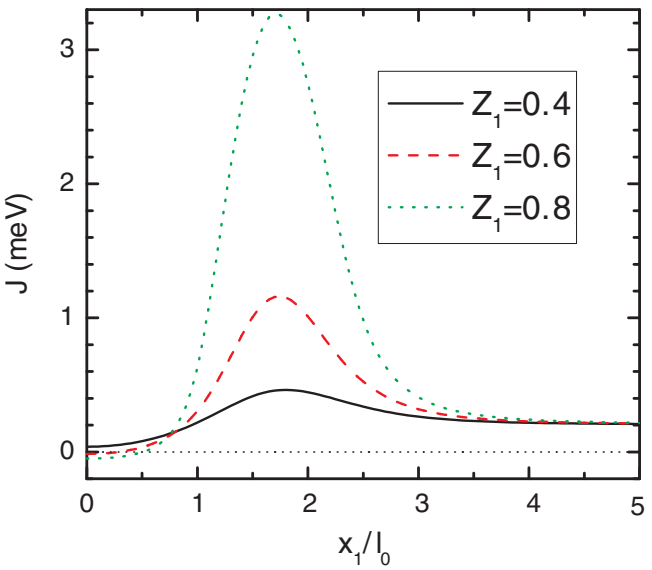

FIG. 25. (Color online) Singlet-triplet spin splitting J as a function of the impurity position along the x axis for different $Z_1 > 0$. The maximum in J is found at different x_1 as Z_1 changes.

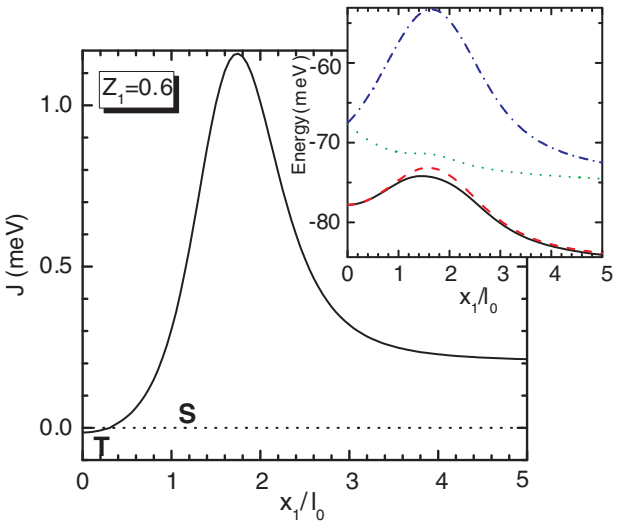

FIG. 26. (Color online) Singlet-triplet spin splitting J as a function of the impurity position along the x axis for a specific case of $Z_1 > 0$: 0.6. Inset is the low-level energy spectrum of the system. As compared with the pronounced anticrossing seen in Fig. 18(b), the $Z_1 = 0.6$ case has the spectrum which is close to having pronounced anticrossings as obtained for $Z_1 = 1$ in Fig. 18(b).

APPENDIX B: HEITLER–LONDON–APPROXIMATION

The closed analytical form of the exchange energy between the two coupled QDs for a single charged impurity located arbitrarily in the xy plane [$\mathbf{R} = (x_0, y_0, 0) l_0$] is obtained by solving a basic two-level problem:

$$
\begin{aligned}
J_{\mathrm{HL}} = -\frac{e^{a_0^2}}{1-e^{4a_0^2}} \Bigg\{ & 2\hbar\omega_0 a_0^2 e^{a_0^2} \\
& + \frac{4V_0\left(e^{\frac{a_0^2-2a_0a_{0x}^2a_8-a_{0x}^2a_8^2}{1+a_{0x}^2}} + e^{\frac{a_0^2+2a_0a_{0x}^2a_8-a_{0x}^2a_8^2}{1+a_{0x}^2}} - 2e^{a_0^2-\frac{a_{0x}^2a_8^2}{1+a_{0x}^2}}\right)}{\sqrt{\left(1+a_{0x}^2\right)\left(1+a_{0y}^2\right)}} \\
& + \frac{4V_b\left(e^{\frac{a_0^2}{1+a_{0bx}^2}} - e^{a_0^2}\right)}{\sqrt{\left(1+a_{0bx}^2\right)\left(1+a_{0by}^2\right)}} + \sqrt{\pi}V_0^C \Bigg[-\sqrt{2}e^{a_0^2} \\
& + \sqrt{2} I_0\left(a_0^2\right) - 4Ze^{a_0^2 - \frac{x_0^2+y_0^2}{2}} I_0\left(\frac{x_0^2+y_0^2}{2}\right) \\
& + 2e^{\frac{a_0^2+2a_0x_0-x_0^2-y_0^2}{2}} Z I_0\left(\frac{a_0^2-2a_0x_0+x_0^2+y_0^2}{2}\right) \\
& + 2e^{\frac{a_0^2-2a_0x_0-x_0^2-y_0^2}{2}} Z I_0\left(\frac{a_0^2+2a_0x_0+x_0^2+y_0^2}{2}\right) \Bigg] \Bigg\}.
\end{aligned}
\tag{B1}
$$

Here, $a_8 = a/l_0$, $a_{0x} = l_0/l_x$, $a_{0y} = l_0/l_y$, $a_{0bx} = l_0/l_{bx}$, and $a_{0by} = l_0/l_{by}$ are dimensionless parameters associated with a series of lengths such as $a, l_x, l_y, l_{bx}, l_{by}$. These parameters, together with depths V_0 and V_b, define the size and the shape of the confinement double well.

The Heitler–London approximation does not allow one to examine the impurity effect on the coupled qubit operations manifested in the mixing of the different singlets and coupling between the singlet-triplet states as already observed and discussed in, e.g., Fig. 18(b). The impurity-position dependence of J_{HL}, as obtained analytically in the last three terms in Eq. (B1), now can be studied in Fig. 23 as a function of x_0. We see that the presence of the charged impurity plays a role only as a weak perturbative interaction to the total energy even in the case when the effective e-I coupling is found to be relatively large (the case $Z_1 = -1$). Such a property like the triplet-singlet transition for a weak repulsive e-I exchange interaction is not found in this case.

APPENDIX C: SINGLET-TRIPLET SPLITTING J FOR INTERMEDIATE IMPURITY EFFECTIVE CHARGES

We show the results obtained for several different intermediate Z_1 for both the negatively and positively charged impurity cases in Figs. 24, 25, and 26. These plots provide a clearer and deeper look into the triplet-singlet transition (Figs. 25 and 26) for a strongly repulsive impurity as well as the physics of anticrossings found in the energy spectrum of the coupled two-dot system. For the $Z_1 < 0$ case, Fig. 24 serves to explain in detail the transition from having a minimum to a maximum in the singlet-triplet splitting J between the two lowest energy levels.

APPENDIX D: SPIN SPLITTING ENERGY OF Si/SiGe COUPLED QUANTUM DOTS

Si QDs have a relatively large effective mass, $m^*_{\mathrm{Si}} \approx 2.8 m^*_{\mathrm{GaAs}}$. Plus, the effective Rydberg energy in Si QDs, as discussed in Sec. II, is higher than the effective Rydberg energy of GaAs QDs. These bring in the fact that the Si QDs have a smaller electron kinetic energy, which means that the electrons tend to be more localized as compared with the case of GaAs. Thus the tunnel rate is expected to be smaller. Our calculations show that for the same model of a coupled two-dot system in which the shape, the size, and the barrier height are kept unchanged: e.g., $V_0 = -50$ meV and $V_b = 30$ meV (corresponding to $\Delta V_b = 9.65$ meV), and the Si/SiGe double-dot system has $\hbar\omega_0 \approx 6.67$ meV ($l_0 \approx 8.48$ nm). The spin singlet-triplet splitting J between the two lowest energy levels in Si/SiGe double dots is found, $J \approx 0.003$ meV, much smaller than the $J \approx 0.204$ meV of the GaAs/AlGaAs double dots. In experiments, the electron tunneling rate in Si/SiGe coupled-double QDs is indeed found to be much lower than the tunneling rate in GaAs/AlGaAs coupled QDs (see, e.g., Ref. 42). In the presence of a charged impurity, e.g., $Z_1 = -0.1$ located at the origin, we obtained J increased to $J \approx 0.008$ meV for Si/SiGe double QDs as compared with $J \approx 0.26$ meV for GaAs/AlGaAs double QDs.

[1]C. H. Bennett and D. P. DiVincenzo, Nature (London) **404**, 247 (2000).
[2]B. E. Kane, Nature (London) **393**, 133 (1998).
[3]D. Loss and D. P. DiVincenzo, Phys. Rev. A **57**, 120 (1998).
[4]R. Vrijen, E. Yablonovitch, K. Wang, H. W. Jiang, A. Balandin, V. Roychowdhury, Tal Mor, and D. P. DiVincenzo, Phys. Rev. A **62**, 012306 (2000).
[5]R. Hanson, L. Kouwenhoven, J. Petta, S. Tarucha, and L. Vandersypen, Rev. Mod. Phys. **79**, 1217 (2007).
[6]J. M. Elzerman, R. Hanson, L. H. Willems van Beveren, B. Witkamp, L. M. K. Vandersypen, and L. P. Kouwenhoven, Nature (London) **430**, 431 (2004).
[7]D. Rugar, R. Budakian, H. J. Mamin, and B. W. Chui, Nature (London) **430**, 329 (2004).
[8]J. R. Petta, A. C. Johnson, A. Yacoby, C. M. Marcus, M. P. Hanson, and A. C. Gossard, Phys. Rev. B **72**, 161301R (2005).
[9]X. Hu and S. Das Sarma, Phys. Rev. A **64**, 042312 (2001).
[10]F. H. L. Koppens, C. Buizert, K. J. Tielrooij, I. T. Vink, K. C. Nowack, T. Meunier, L. P. Kouwenhoven, and L. M. K. Vandersypen, Nature (London) **442**, 766 (2006).
[11]M. Ciorga, A. S. Sachrajda, P. Hawrylak, C. Gould, P. Zawadzki, S. Jullian, Y. Feng, and Z. Wasilewski, Phys. Rev. B **61**, R16315 (2000).
[12]J. M. Elzerman, R. Hanson, J. S. Greidanus, L. H. Willems van Beveren, S. De Franceschi, L. M. K. Vandersypen, S. Tarucha, and L. P. Kouwenhoven, Phys. Rev. B **67**, 161308(R) (2003).
[13]M. Poiro-Ladrière, M. Ciorga, J. Lapointe, P. Zawadzki, M. Korkusinski, P. Hawrylak, and A. S. Sachrajda, Phys. Rev. Lett. **91**, 026803 (2003).
[14]J. R. Petta, A. C. Johnson, C. M. Marcus, M. P. Hanson, and A. C. Gossard, Phys. Rev. Lett. **93**, 186802 (2004).
[15]W. Tittel, J. Brendel, H. Zbinden, and N. Gisin, Phys. Rev. Lett. **81**, 3563 (1998).
[16]G. Weihs, T. Jennewein, C. Simon, H. Weinfurter, and A. Zeilinger, Phys. Rev. Lett. **81**, 5039 (1998).
[17]G. Burkard, D. Loss, and D. P. DiVincenzo, Phys. Rev. B **59**, 2070 (1999).
[18]D. Loss and E. V. Sukhorukov, Phys. Rev. Lett. **84**, 1035 (2000).
[19]M. A. Rowe, D. Kielpinski, V. Meyer, C. A. Sackett, W. M. Itano, C. Monroe, and D. J. Wineland, Nature (London) **409**, 791 (2001).
[20]X. Hu and S. Das Sarma, Phys. Rev. B **69**, 115312 (2004).
[21]G. Burkard, J. Phys. Condens. Matter **19**, 233202 (2007).
[22]X. Hu and S. Das Sarma, Phys. Rev. A **61**, 062301 (2000).
[23]R. de Sousa, X. Hu, and S. Das Sarma, Phys. Rev. A **64**, 042307 (2001).
[24]J. Levy, Phys. Rev. Lett. **89**, 147902 (2002).
[25]A. Harju, S. Siljamäki, and R. M. Nieminen, Phys. Rev. Lett. **88**, 226804 (2002).
[26]R. Hanson, L. H. Willems van Beveren, I. T. Vink, J. M. Elzerman, W. J. M. Naber, F. H. L. Koppens, L. P. Kouwenhoven, and L. M. K. Vandersypen, Phys. Rev. Lett. **94**, 196802 (2005).
[27]J. R. Petta, A. C. Johnson, J. Taylor, E. A. Laird, A. Yacoby, M. D. Lukin, C. M. Marcus, M. P. Hanson, and A. C. Gossard, Science **309**, 2180 (2005).
[28]I. van Weperen, B. D. Armstrong, E. A. Laird, J. Medford, C. M. Marcus, M. P. Hanson, and A. C. Gossard, e-print arXiv:1101.5654v3 (unpublished).
[29]I. P. Gimenez, C. Y. Hsieh, M. Korkusinski, and P. Hawrylak, Phys. Rev. B **79**, 205311 (2009).
[30]W. G. van der Wiel, S. De Franceschi, J. M. Elzerman, T. Fujisawa, S. Tarucha, and L. P. Kouwenhoven, Rev. Mod. Phys. **75**, 1 (2002).
[31]J. R. Petta, J. M. Taylor, A. C. Johnson, A. Yacoby, M. D. Lukin, C. M. Marcus, M. P. Hanson, and A. C. Gossard, Phys. Rev. Lett. **100**, 067601 (2008).
[32]Q. Li, L. Cywiński, D. Culcer, X. Hu, and S. Das Sarma, Phys. Rev. B **81**, 085313 (2010).
[33]The minimum in J varies when V_b changes. Therefore, the minimal splitting energy for $V_b = 13$ meV is found at a different position of the impurity as compared with the "standard" $\approx 2l_0$ for the case $V_b = 30$ meV
[34]E. H. Hwang and S. Das Sarma, Phys. Rev. B **77**, 235437 (2008).
[35]L. A. Tracy, E. H. Hwang, K. Eng, G. A. Ten Eyck, E. P. Nordberg, K. Childs, M. S. Carroll, M. P. Lilly, and S. Das Sarma, Phys. Rev. B **79**, 235307 (2009).
[36]C. Marcus and A. Yacoby (private communication).
[37]X. Hu and S. Das Sarma, Phys. Rev. Lett. **96**, 100501 (2006); M. Stopa and C. M. Marcus, Nano Lett. **8**, 1778 (2008).
[38]D. Culcer, X. Hu, and S. Das Sarma, Appl. Phys. Lett. **95**, 073102 (2009).
[39]C. Nayak, S. H. Simon, A. Stern, M. Freedman, and S. Das Sarma, Rev. Mod. Phys. **80**, 1083 (2008).
[40]Madhu Thalakulam, C. B. Simmons, B. M. Rosemeyer, D. E. Savage, M. G. Lagally, Mark Friesen, S. N. Coppersmith, and M. A. Eriksson, Appl. Phys. Lett. **96**, 183104 (2010).
[41]K. Ono and S. Tarucha, Phys. Rev. Lett. **92**, 256803 (2004).
[42]I. S. Gradshteyn, I. M. Ryzhik, A. Jeffrey, and D. Zwillinger, *Tables of Integrals, Series, and Products*, 6th ed. (Academic, San Diego, 2000).